IEEE Access
Multidisciplinary | Rapid Review | Open Access Journal

Received 18 November 2023, accepted 3 December 2023, date of publication 7 December 2023,
date of current version 19 January 2024.

Digital Object Identifier 10.1109/ACCESS.2023.3340313

RESEARCH ARTICLE

Validation of Sliding Mode and Passivity Control in High-Power Quadratic Buck Converter Through Rapid Prototyping

RAFAEL ANTONIO ACOSTA-RODRÍGUEZ[1], (Member, IEEE),
FREDY HERNÁN MARTINEZ-SARMIENTO[2], (Member, IEEE),
GERMAN ARDUL MÚÑOZ-HERNANDEZ[3], (Senior Member, IEEE),
GERARDO MINO-AGUILAR[3], (Senior Member, IEEE),
EDGAR ALFREDO PORTILLA-FLORES[4], (Member, IEEE),
PAOLA ANDREA NIÑO-SUAREZ[4], (Member, IEEE),
AND OCTAVIO JOSÉ SALCEDO-PARRA[5], (Member, IEEE)

[1]Smart Internet Research Group, ARMOS Group Colciencias, Universidad Distrital Francisco José of Caldas, Bogotá 111611, Colombia
[2]ARMOS Group Colciencias, Universidad Distrital Francisco José of Caldas, Bogotá 111611, Colombia
[3]Faculty of Electronic Sciences, Meritorious Autonomous University of Puebla (BUAP), Puebla 72592, Mexico
[4]Center for Innovation and Technological Development in Computing (CIDETEC), Instituto Politécnico Nacional (IPN), Tlaxcala 07738, Mexico
[5]Smart Internet Research Group Colciencias, Universidad Distrital Francisco José of Caldas, Bogotá 111611, Colombia

Corresponding author: Rafael Antonio Acosta-Rodríguez (raacostar@udistrital.edu.co)

This work was supported in part by the Universidad Distrital Francisco José of Caldas, Bogotá, Colombia, through the Smart Internet Research Group; in part by the Ph.D. Internship with the National Polytechnic Institute (IPN), approved as a research stay in the DISRYM Program, CDMX, December 01, 2021; in part by the Doctorate in Robotic and Mechatronic Systems Engineering; and in part by a research professors, facilities, and laboratories of the Meritorious Autonomous University of Puebla (BUAP), Mexico, through PNPC of CONACYT, Puebla, under Grant C.P. 72570.

ABSTRACT This document introduces a rapid control prototyping (RCP) approach applied to the industrial sector using a non-linear Quadratic Buck Converter (QBC) DC-DC. The goal is to reduce manufacturing costs for materials and electronic devices while enhancing the power quality in the system's response. An experimental setup is utilized to create a functional model, converting 380 VDC to 48 VDC at a power level of 500 W. dSPACE CP1103 is employed to implement Model in the Loop (MIL), Software in the Loop (SIL), and Hardware in the Loop (HIL) simulations. Modern control techniques, including sliding mode control (SMC) and passivity-based control (PBC), are employed to devise a robust control scheme capable of maintaining stability in real-time (RT) and resisting disturbances. The document concludes with a performance analysis, PI, Cp, CpK, Z-score, and ITAE considering response time, signal accuracy, system stability, and resource utilization efficiency.

INDEX TERMS dSPACE, hardware in the loop (HIL), model in the loop (MIL), passivity control, performance indices, quadratic buck converter (QBC), rapid control prototyping (RCP), real-time (RT), sliding mode control, software in the loop (SIL).

I. INTRODUCTION

A. MOTIVATION AND BACKGROUND

Recent advancements in the design and development of DC converters have introduced features like dual modes of operation, DC ports, high voltage gain ratios, bi-directional conversion capabilities, and enhanced efficiency [1], [2], [3], [4]. These innovations play a pivotal role in advancing energy conversion technologies, with the potential to benefit a wide range of applications, including renewable energy, energy storage systems, and power electronics [1], [2], [3], [4].

The associate editor coordinating the review of this manuscript and approving it for publication was Diego Bellan.

Within the realm of power conversion, there have been notable developments in various techniques and topologies for direct current (DC) to direct current (DC) converters. These advancements aim to meet the growing demands for efficiency and flexibility across diverse applications. Notably, the design of transformer less converters has witnessed significant progress, offering advantages such as reduced size, weight, and cost. Among these innovations, the transformer less DC/DC converter with dual modes of operation and continuous input current port has emerged [1]. Additionally, a novel transformer-less quadratic buck-boost converter, featuring a high voltage gain ratio and continuous input/output current ports, has been proposed [2]. These converter designs exhibit marked improvements in terms of efficiency and performance compared to conventional topologies.

In the context of direct current to alternating current (AC) conversion, a four-quadrant buck converter with a common ground has been developed [3]. This topology facilitates bidirectional conversion between DC and AC, proving especially beneficial in renewable energy applications and energy storage systems. Finally, a non-isolated DC-DC converter with dual operating modes and a positive voltage output has been introduced [4]. This innovation offers enhanced flexibility and efficiency for power conversion in specific applications.

Traditional converter design and manufacturing processes demand extensive time investment in physical tests, measurements, and experimental verification for each component of a quadratic converter [5]. Consequently, mass production becomes a more complex and time-consuming endeavor [6], [7].

Moreover, the study and validation of modern control techniques for quadratic converters, characterized by their nonlinear behavior, involve numerous steps lacking a well-defined methodological framework. This often results in a significant time investment for study validation, discouraging implementation by trial and error [8].

The adoption of rapid prototyping methodologies opens new avenues for optimizing industrial processes. It allows for efficient programming of simulations, preventing unnecessary expenditure of time, components, and raw materials. Additionally, it ensures real-time monitoring of the plant's operation and offers excellent control response to disturbances through its SIL tool [9].

Rapid prototyping with dSPACE refers to leveraging dSPACE-branded hardware-in-the-loop (HIL) systems for the early development and validation of electronic and control systems across various industries, including automotive and aerospace [9].

dSPACE, a renowned company, offers simulation and testing tools and solutions for electronic and control system development. Their HIL systems enable real-time emulation of electronic component behavior, facilitating the evaluation of systems in a virtual environment before real-world implementation [9].

The application of dSPACE for rapid prototyping involves creating virtual prototypes of complex systems, such as vehicle control systems, propulsion systems, or avionics systems. These virtual prototypes empower engineers to develop and validate control algorithms, conduct functional tests, and assess system performance within a secure and controlled environment [9].

By harnessing dSPACE for rapid prototyping, engineers can expedite development processes, reduce costs, and mitigate risks associated with real-world system deployment. Moreover, dSPACE offers a wide array of tools and models for development and simulation, simplifying the creation of sophisticated and accurate virtual prototypes [9].

The rapid prototyping methodology facilitates the determination of optimal device values in the design of the quadratic converter topology. This involves considerations of efficiency, availability, performance, and economy, as well as the selection and construction of coils suitable for the circuit. Furthermore, this methodology contributes to precise parameter adjustment for operating points and equilibrium points, even in the presence of disturbances during the proposed control implementation [8], [9].

B. LITERATURE REVIEW

The equations of the nonlinear model [8] must be adjusted to achieve the required parameterization. This adjustment aims to simplify the creation of an assembly standard from the model, thereby facilitating cost savings in implementation, manufacturing, and extensive laboratory testing.

Furthermore, by employing and configuring an acquisition card such as FPGA, Arduino, Raspberry Pi, DSP, or dSPACE, a control implementation dynamic can be established to provide PWM (Pulse Width Modulation) by the plant's physical requirements [9]. The application of rapid prototyping with dSPACE entails the utilization of dSPACE's hardware-in-the-loop (HIL) systems to create virtual prototypes of electronic and control systems. This approach empowers engineers to develop, validate, and optimize their systems before real-world implementation [9]. This digital treatment is essential as it involves signal discretization tailored to the plant's characteristics. Such digital handling ensures easy system control and monitoring in real-time (RT), preventing device saturation and overheating, which can lead to energy losses or system malfunction.

It is essential to consider that the control strategy originates from the initial design of the mathematical model. This mathematical model determines an averaged model, which, despite having a fourth-order dynamic with right-sided zeros, poses significant challenges when using a single control loop. However, thanks to the concept of (RCP), both a non-linear model and a linear model for this class of converters are derived, along with a methodology for designing a controller. While control techniques have been widely applied to DC-DC converters, the influence of the current loop on their dynamic behavior has been documented, resulting in a transition from second-order to first-order dynamics. Yet, this effect is less clear in the case of more complex topologies [11], such as

cascaded converters, where right-sided zeros arise due to internal coupling.

In the realm of electronic circuits, certain switched power Buck converters play a vital role in generating voltage and current with characteristics that ensure power supply from a power source [12], [13]. These DC-DC converters are responsible for adapting the signal to the desired continuous values [14].

Both the controller and the plant can be simulated in real-time using the same simulator, SIL holds an advantage over RCP and HIL as it preserves signal integrity by not using any inputs or outputs. Additionally, both the controller and plant models run on the same simulator [15]. These converters are positioned between a primary source and a load, which, in some cases, is modeled as a power load. The input comprises direct voltage loads that can power various digital electronic devices, with a control loop governing the commutator element's conductance time. This improvement enhances transit and stabilizes the system against disturbances [6], [7], [12], [14], [16].

The system exhibits non-linear behavior due to its variable structure. During its study, non-linear control techniques, such as the passivity-based control (PBC) technique and sliding mode control (SMC), are applied, and validated in the presence of time-varying disturbances [17], [18].

Our proposed approach ensures the control of the system's non-linear dynamics through the (RCP) methodology, based on the SIL technique. This methodology runs the entire program in the destination environment, with monitoring conducted through the MIL and development embedded in an acquisition card or microprocessor via the HIL concept. The process begins with emulating the direct current QBC, continues through its initial construction, and culminates in obtaining its control strategy. Thus, this methodology allows the plant's design, based on intelligent device selection, to guarantee optimal operating parameters. This is achieved through control models founded on the study of the system's non-linear behavior, validation of control strategies, and configuration of appropriate dynamics for specific operating points using real-time (RTS) embedded systems [15].

This work showcases the development of an electronic nonlinear system aimed at controlling direct current commutated converters. It emphasizes the utilization of nonlinear control techniques from modeling to final implementation. Its significance in controlling various types of systems opens opportunities for optimizing various electrical industrial processes, preventing unnecessary energy expenses, enhancing safety, reducing implementation time, improving response speed, and ensuring ease of electrical transfer control [15].

To validate the optimization of control system performance, the Integral Time Index of Absolute Error (ITAE) is employed. This choice is due to its ability to provide precise temporal measurements of system response.

The Integral Time of Absolute Error (ITAE) index is widely regarded as the most suitable index for use in a quadratic loop [19], [20]. This preference arises because ITAE exhibits higher sensitivity to significant errors while maintaining lower sensitivity to minor errors, making it particularly suitable for systems where the avoidance of large errors is paramount [21].

ITAE serves as a measure of error in process control over time, rooted in the integration of the absolute error over time [22]. It offers a means of assessing control stability and accuracy, demonstrating sensitivity to changes in system response time, making it valuable for detecting system changes that may impact control performance [23].

Importantly, ITAE serves as a performance measure that remains independent of the system's operational point. This quality enables comparisons of control performance across different operational points. Furthermore, ITAE proves robust in the presence of system noise, facilitating the evaluation of control performance in noisy conditions. It also enables the optimization of controller parameters, as proper tuning can minimize ITAE. ITAE's significance in switching converter control is attributed to its ability to accurately assess control performance over time, sensitivity to changes in system response time, independence from the operating point, and robustness in the presence of system noise [22].

C. CONTRIBUTION AND PAPER ORGANIZATION

This document is constituted as follows:

Mathematical Modeling: Section II presents the development of comprehensive mathematical models for the dynamic QBC system, incorporating variable representations and state equations.

System Behavior Understanding: In Section III, a switched model is introduced to comprehend how the system behaves in different states. The variable "u" is utilized as an input or control signal to modulate system behavior and achieve desired responses.

Steady-State Analysis: Section IV focuses on the average model, describing the dynamic behavior of the periodic system, with a specific emphasis on steady-state analysis.

Control System Design: Section V explores the linearization of the system as a tool for designing real-time automatic control systems capable of handling complex systems. This design is based on the plant's transfer function.

Construction Equations: Section VI formulates construction equations for the quadratic Buck converter during static design. It considers parameters such as the duty cycle to precisely determine device values for constructing the plant. Validation of outputs and their performance is carried out.

Sliding Mode Control (SMC): In Section VII, sliding mode control (SMC) is developed to stabilize non-linear systems with complex dynamics and unknown variables. This includes the design of a controller and compensator type II, with performance evaluation through simulations and subsequent experimental validation.

Passivity-Based Control: Section VIII introduces passivity-based control. This control strategy is designed to ensure that

the converter output voltage tracks a desired reference while minimizing energy storage. It effectively reduces the impact of load voltage fluctuations and disturbances on the system. The section also investigates error dynamics and passive output feedback for precise error control and assesses control system accuracy under various disturbances and operating conditions.

Canonical Forms: Section IX applies canonical forms to the QBC for designing passive systems and controllers. This approach facilitates the systematic analysis and design of linear dynamic systems and enables the creation of controller designs. It involves the implementation of control loops based on passive canonical forms, aiming for convergence to desired reference signals.

Experimental Development: Section X presents the experimental development in two parts. First, it covers the development of the PCB printed circuit and the assembly of the QBC or system plant. Second, it delves into the design of rapid prototyping using the dSPACE 1103, incorporating control slider mode control and passivity-based control in the converter. These controls are validated in a simulated environment using Control Desk, which is employed for the development and configuration of real-time control systems before experimental testing with electrical response analysis on an oscilloscope.

This document offers a comprehensive exploration of the dynamic QBC system, encompassing mathematical modeling, control strategy development (including both SMC and passivity-based control), and rigorous experimental validation. The primary objective is to enhance system stability, minimize energy storage, and achieve precise control even in the presence of disturbances and varying operating conditions. The subsequent analysis of results in Section XI, where the methodological process that determines is presented the analysis reveals strong control performance, as indicated by low Multiplied Time Integral Absolute Error (ITAE) values for various variables. Notably, for vc1, sliding mode control achieves '1.02e-03', and passivity-based control records '1.93e-01'. In iL1, sliding mode control SMC attains '3.90e-05', while passivity-based control reaches '1.65e-02'. for iL2, sliding mode control SMC registers '1.76e-04', and passivity-based control exhibits '3.15e-02'. Lastly, for Vc2, sliding mode control SMC records '1.34e-06', and passivity-based control achieves '1.05e-02'. These findings underscore the stability and efficacy of the control strategies, providing valuable insights for practical applications, and the key conclusions drawn in Section XII provide valuable insights into the effectiveness of these control strategies and their potential practical applications.

II. QUADRATIC BUCK SWITCHED CONVERTER MODEL

According to the quadratic Buck circuits generated by the MATLAB program, as can be seen in Figure 1 the ON state, and the OFF state, are obtained in figure 1.

The equations that model the QBC are described below.

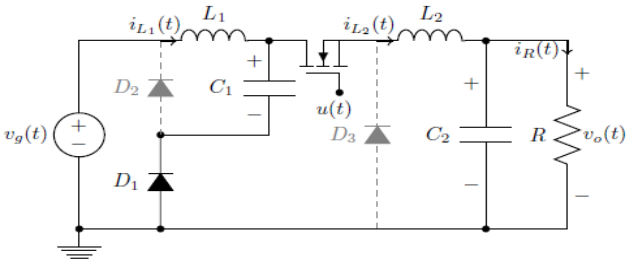

FIGURE 1. Quadratic Buck in ON state.

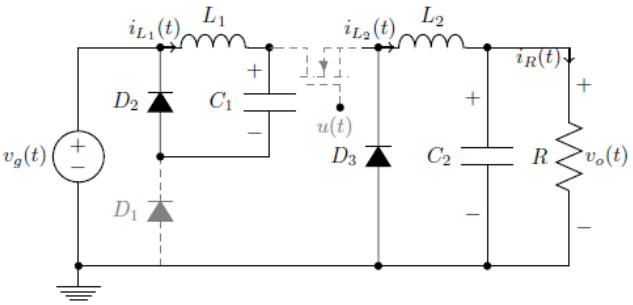

FIGURE 2. Quadratic Buck in OFF state.

A. REPRESENTATION OF THE EQUATIONS IN STATE ON

Behavior in the ON state, according to figure 1, the following equations are obtained:

$$V_g = V_{L1} + V_{C1} \tag{1}$$
$$V_{C1} = V_{L2} + V_{C2} \tag{2}$$
$$I_{L1} = V_{C1} + I_{L2} \tag{3}$$
$$I_{L2} = I_{C2} + I_R \tag{4}$$

Representing the previous equations in state variables, equation (1) is written as follows:

$$\frac{d_{iL1}}{dt} = \frac{V_g - v_{C1}}{L_1} \tag{5}$$

Similarly, we obtain equation (2)

$$\frac{d_{iL2}}{dt} = \frac{v_{C1} - v_{C2}}{L_2} \tag{6}$$

For equation (3)

$$\frac{d_{VC1}}{dt} = \frac{I_{L1} - I_{L2}}{C_1} \tag{7}$$

and finally for equation (4)

$$\frac{d_{VC2}}{dt} = \frac{I_{L2} - I_R}{C_2} \tag{8}$$

B. REPRESENTATION OF THE EQUATIONS IN STATE OFF

According to the OFF state, of the quadratic Buck, according to figure 2, the following equations are obtained:

$$V_{L1} = -v_{C1} \tag{9}$$
$$V_{L2} = -v_{C2} \tag{10}$$
$$I_{L1} = -I_{C1} \tag{11}$$
$$I_{L2} = I_{C2} + I_R \tag{12}$$

When representing the previous equations from 9 to 12, using state variables, it is obtained for equation (9).

$$\frac{d_{iL1}}{dt} = \frac{-v_{C1}}{L_1} \tag{13}$$

For equation (10), we have:

$$\frac{d_{iL2}}{dt} = \frac{-v_{C2}}{L_2} \tag{14}$$

Similarly in equation (11)

$$\frac{d_{VC1}}{dt} = \frac{i_{L1}}{C_1} \tag{15}$$

And finally for equation (12)

$$\frac{d_{VC2}}{dt} = \frac{i_{L2} - i_R}{C_2} \tag{16}$$

III. QUADRATIC BUCK SWITCHED MODEL

The equation of the state variable is multiplied obtaining in the ON state by U and in the OFF state by (1-U).

For $\mathbf{I_{L1}}$, in this case, the state variable is obtained by the following equation:

$$\frac{d_{iL1}}{dt} = \frac{V_g - v_{C1}}{L_1} * u + \frac{-v_{C1}}{L_1} * (1-u) \tag{17}$$

$$\frac{d_{iL1}}{dt} = \frac{V_g}{L_1} * u - \frac{v_{C1}}{L_1} \tag{18}$$

For I_{L2}, the state variable is obtained from the equation:

$$\frac{d_{iL2}}{dt} = \frac{v_{C1} - v_{c2}}{L_2} * u + \frac{-v_{c2}}{L_2} * (1-u) \tag{19}$$

$$\frac{d_{iL2}}{dt} = \frac{v_{C1}}{L_2} * u - \frac{v_{c2}}{L_2} \tag{20}$$

For the variable v_{C1} we obtain:

$$\frac{d_{VC1}}{dt} = \frac{i_{L1} - i_{L2}}{C_1} * u + \frac{I_{L1}}{C_1} * (1-u) \tag{21}$$

$$\frac{d_{VC1}}{dt} = \frac{-i_{L2}}{C_1} * u + \frac{i_{L2}}{C_1} \tag{22}$$

For the state variable v_{C2} we obtain:

$$\frac{d_{VC2}}{dt} = \frac{i_{L2} - i_R}{C_2} * u + \frac{i_{L2} - i_R}{C_2} * (1-u) \tag{23}$$

$$\frac{d_{VC2}}{dt} = \frac{i_{L2}}{C_2} * u - \frac{v_{c2}}{C_2 R} \tag{24}$$

IV. AVERAGE MODEL QUADRATIC BUCK

Changing the variable u to d, and naming the equations of state as functions:

For the variable $\mathbf{iL_1}$

$$f_1 = \frac{d_{iL1}}{dt} = \frac{V_g}{L_1} * d - \frac{v_{C1}}{L_1} \tag{25}$$

for the variable iL_2

$$f_2^I = \frac{d_{iL2}}{dt} = \frac{v_{C1}}{L_2} * d - \frac{v_{c2}}{L_2} \tag{26}$$

for the variable v_{C1}

$$f_3 = \frac{d_{VC1}}{dt} = \frac{-i_{L2}}{C_1} * d + \frac{i_{L1}}{C_1} \tag{27}$$

$$f_4 = \frac{d_{VC2}}{dt} = \frac{i_{L2}}{C_2} * d - \frac{v_0}{C_2 * R} \tag{28}$$

Equating the previously given equations to zero, the following is obtained:

$$f_1 = \frac{V_g}{I_1} * d - \frac{V_{C1}}{L_1} = 0 \tag{29}$$

Reducing we get:

$$V_g * D = V_{C1} \tag{30}$$

For the function f_2

$$f_2 = \frac{V_{C1}}{I_2} * d - \frac{V_0}{L_2} = 0 \tag{31}$$

Simplifying:

$$f_2 = V_{C1} * D = V_0 \tag{32}$$

For the function f_3 We have:

$$f_3 = \frac{-I_{L2}}{C_1} * d + \frac{I_{L1}}{C_1} = 0 \tag{33}$$

Simplifying:

$$I_{L2} * D = I_{L1} \tag{34}$$

and finally for the function f_4

$$f_4 = \frac{I_{L2}}{C_2} - \frac{V_{c2}}{C_2 * R} = 0 \tag{35}$$

Simplifying, the formula is obtained:

$$I_{L2} = \frac{V_0}{R} \tag{36}$$

V. QUADRATIC BUCK LINEAR MODEL

Its main objective through the model provide the Transfer Function that describes the behavior of the system, obtaining the following matrix:

$$\frac{d}{dt} = \begin{bmatrix} i_{L1} \\ v_{C1} \\ i_{L2} \\ v_{C2} \end{bmatrix} = Ax + Bu$$

$$A = \begin{bmatrix} \frac{\partial}{\partial iL_1} f_1 & \frac{\partial}{\partial iC_1} f_1 & \frac{\partial}{\partial iL_2} f_1 & \frac{\partial}{\partial vC_2} f_1 \\ \frac{\partial}{\partial iL_1} f_2 & \frac{\partial}{\partial iC_1} f_2 & \frac{\partial}{\partial iL_2} f_2 & \frac{\partial}{\partial vC_2} f_2 \\ \frac{\partial}{\partial iL_1} f_3 & \frac{\partial}{\partial iC_1} f_3 & \frac{\partial}{\partial iL_2} f_3 & \frac{\partial}{\partial vC_2} f_3 \\ \frac{\partial}{\partial iL_1} f_4 & \frac{\partial}{\partial iC_1} f_4 & \frac{\partial}{\partial iL_2} f_4 & \frac{\partial}{\partial vC_2} f_4 \end{bmatrix} * \begin{bmatrix} \widehat{iL_1} \\ \widehat{vC_1} \\ \widehat{iL_2} \\ \widehat{vC_2} \end{bmatrix}$$

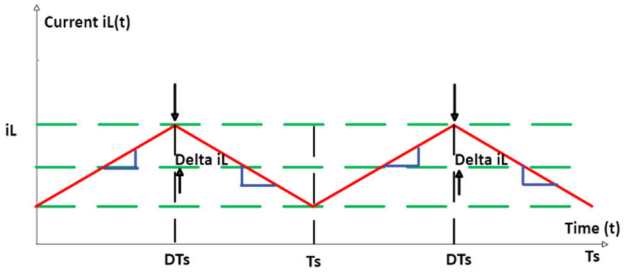

FIGURE 3. Voltage delta ripple in coils.

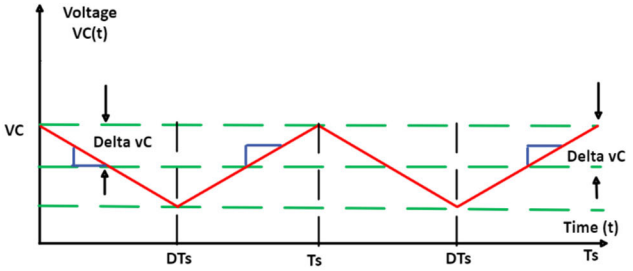

FIGURE 4. Ripple current in the capacitor.

$$Bu = \begin{bmatrix} \frac{\partial}{\partial d} f_1 \\ \frac{\partial}{\partial d} f_2 \\ \frac{\partial}{\partial d} f_3 \\ \frac{\partial}{\partial d} f_4 \end{bmatrix} * \widehat{d} \qquad Y = \begin{bmatrix} 0 & 0 & 0 & 1 \end{bmatrix} * \begin{bmatrix} \widehat{\iota L_1} \\ \widehat{vC_1} \\ \widehat{\iota L_2} \\ \widehat{vC_2} \end{bmatrix}$$

The transfer function is given by the formula:

$$G(s) = Y * [SI - A]^{-1} * Bu \tag{37}$$

Solving equation 37, the transfer function $G(s)$ is (38), as shown at the bottom of the page.

VI. QBC STATIC DESIGN

Inductances: According to the shape of the current ripple in the coil, the general equation for the value of the inductance is defined, as can be seen in Figure 3 Where the slope of the line from 0 to $\boldsymbol{DT_s}$ is the inductance equation in the ON state, there is the slope between $\boldsymbol{DT_s}$ *and* $\boldsymbol{T_s}$ is the value of the coil current in the OFF state by definition of slope

$$\boldsymbol{m} = \frac{\boldsymbol{\Delta Y}}{\boldsymbol{\Delta X}} \tag{39}$$

From there we can find the value of each of the coils.

L_1 : To find this inductor according to equation (5) and equation (39), where:

$$\frac{V_g - v_{C1}}{L_1} = \frac{2 * \Delta I}{D * TS}$$

clearing L_1: we have

$$\frac{D * TS * (V_g - v_{C1})}{2 * \Delta I} \tag{40}$$

Which can be reduced by equation (30) in:

$$L_1 = \frac{D * TS * V_g(1 - v_{C1})}{2 * \Delta I} \tag{41}$$

$\boldsymbol{L_1}$: To find it, the ON state is used, according to equation (6) and equation (39).

$$\frac{v_{C1} - v_{C2}}{L_2} = \frac{2 * \Delta I}{D * TS}$$

clearing L_2: we have

$$L_2 = \frac{D * TS * (v_{C1} - v_{C2})}{2 * \Delta I} \tag{42}$$

According to equation (32), the equation can be reduced to:

$$L_2 = \frac{D * TS * v_{C1}(1 - D)}{2 * \Delta I} \tag{43}$$

Capacitances: According to Figure 4, it can be analyzed that, according to the ripple for the calculation of capacitance, the shape of the current ripple varies slightly, starting with a negative slope.

In the same way, the state of the coil is multiplied by the ON state, however, in Figure 3 it is observed as part of the OFF state; but in this case, it varies slightly, since it starts with a negative slope when multiplying the equation by less indicating that the slope is negative, the same calculation is for the slope.

$\boldsymbol{C_1}$: To find the value of the capacitor $\boldsymbol{C_1}$, using the ON state, according to equation (6) and equation (39).

$$\frac{v_{C1} - v_{C2}}{L_2} = \frac{2 * \Delta I}{D * TS}$$

Solving C_1 from the equation:

$$C_1 = \frac{D * TS * (I_{L1} - I_{L2})}{2 * \Delta v_{C1}} \tag{44}$$

Using equation (34), the equation is reduced to:

$$C_1 = \frac{-D * TS * I_{L1}(1 - I_{L2})}{2 * \Delta v_{C1}} \tag{45}$$

C_2 : To find the value of the capacitor C_2 using the ON state according to equation (8) and equation (39), where:

$$\frac{I_{L2} - I_R}{C_2} = \frac{2 * \Delta v_{C2}}{D * TS}$$

Solving C_2 the previous equation we get:

$$C_2 = \frac{D * TS * (i_{L2} - i_R)}{2 * \Delta V_{C2}} \tag{46}$$

Using equation (36), this equation can be reduced.

$$G(s) = \frac{\left(\left(\frac{v_{C1}}{C_1 C_2 L_2}\right)\left(S^2 - \left(\frac{D_{IL1L1}}{V_{C1}}\right)S + \left(\frac{1}{L_1} + \frac{D_{vg}}{R_{C1} V_{C1}}\right)\right)\right)}{S^4 + \left(\frac{1}{RC_2}\right)S^3 + \left(\frac{D^2 L_1 + L_2 - 2}{L_1 L_2}\right)S^2 + \left(\frac{D^2 L_1 + L_2}{C_1 C_2 L_1 L_2 R}\right)S + \left(\frac{1}{C_1 C_2 L_1 L_2 R}\right)} \tag{38}$$

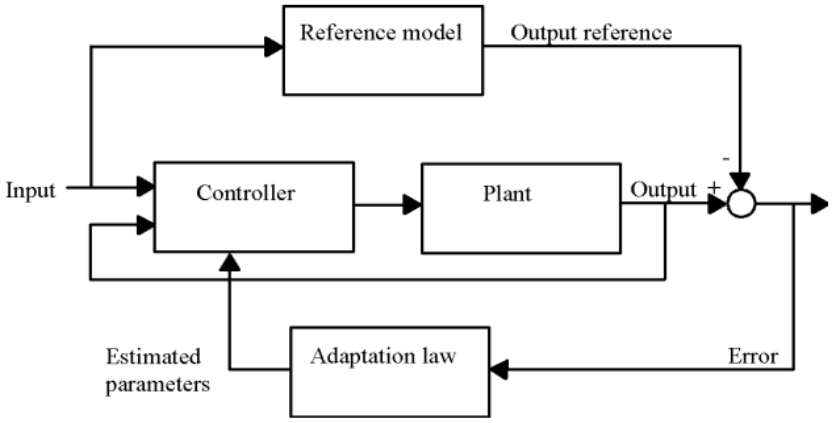

FIGURE 5. Proposed control structure scheme for the quadratic buck converter.

to:

$$C_2 = 0 \tag{47}$$

Since the value of $\boldsymbol{C_2}$ cancels, it can be experimentally demonstrated that it works correctly with the value of $\boldsymbol{C_1}$

A. DUTY CYCLE

Being considered very useful for the handling of the switched PWM signal sources, in the task of activating or deactivating the transistors; for this, equations (30) and (31) are equalized, obtaining:

$$V_g * D = \frac{v_0}{D} \tag{48}$$

clearing D

$$D = \sqrt{\frac{v_0}{V_g}} \tag{49}$$

VII. QBC SLIDING MODE CONTROL DESIGN SMC

The main characteristic of the sliding mode control SMC is to achieve an independent response concerning the system parameters, for this reason, the plant of the QBC is specially adapted, and it is controllable because each state variable can be affected by an input signal. The output voltage and its derivative are continuous and accessible for measurement. In practice with DC-DC converters, the rate of movement of the input current is much faster than the rate of movement of the output voltage. This control problem can be solved by using a control structure.

with two combined control loops as shown in Figure 5, which can be represented as an inner current control loop and an outer voltage control loop [24].

When the control by the current in the inductors is carried out, the hysteresis control is used, and in the same way, the case of control by voltage is developed, in which nonlinear control techniques are implemented, with the two approaches there is an implementation in the various types of converters such as Buck, Boost, or Buck-Boost [25], [26], [27], [28].

A. DESCRIPTION OF THE SLIDER MODE CONTROL IN THE DC-DC QBC, SWITCHED MODEL

The equations of state that represent the conditions of the variables for the conditions of the system are expressed below, according to the control law in which the system is expressed through the differential equations corresponding to the vector field:

$$\frac{d_{i1}}{dt} = \frac{-v_1}{L_1} + \frac{V_g}{L_1}u \tag{50}$$

$$\frac{d_{v1}}{dt} = \frac{i_1}{C_1} - \frac{i_2}{C_1}u \tag{51}$$

$$\frac{d_{i2}}{dt} = \frac{v_1}{L_2}u + \frac{v_2}{L_2} \tag{52}$$

$$\frac{d_{v2}}{dt} = \frac{i_2}{C_2} - \frac{v_{C2}}{R_{C1}} \tag{53}$$

where the value of V_{C2} must be less than V_{C1}, and in turn less than V_g

$$V_{C2} < V_{C1} < V_g \tag{54}$$

The dynamics of the system in sliding mode control are described. Therefore, the existence of the sliding mode the control condition is satisfied, and a stable system is obtained by choosing a the positive value of the current as a system reference.

$$S(x) = i_1(t) - i_{ref}(t)$$

$$S(x) = 0 \quad \dot{S}(x) = 0 \tag{55}$$

$$i_1(t) = i_{ref}(t) \tag{56}$$

$$\frac{d_{i1}}{dt} = \frac{d_{iref}}{dt}$$

$$\frac{-v_1}{L_1} + \frac{v_g}{L_1}u = \frac{d_{iref}}{dt} \tag{57}$$

$$u_{eq} = \frac{L_1}{v_g}\left(\frac{d_{iref}}{dt} + \frac{v_1}{L_1}\right) \tag{58}$$

$$0 < u_{eq} < 1$$

$$u_{eq} = \frac{L_1}{v_g}i_{ref} + \frac{v_1}{v_g} \tag{59}$$

According to the equations, the control law is chosen assuming that equation (86) is greater than zero, in a neighborhood of S, the necessary condition for a sliding regime to exist, is that the polynomial inequality is validated as an open neighborhood s.

$$0 < \frac{L_1}{v_g}\left(i_{ref} + \frac{v_1}{L_1}\right) < 1 \tag{60}$$

Under the assumption that (87), around S, it is easy to see that this given existence condition is also sufficient.

$$0 < \frac{L_1}{v_g} i_{ref} + \frac{v_1}{L_1} < 1 \tag{61}$$

Replacing the condition of the law in the state variables, we obtain:

$$\begin{aligned}
\frac{d_{v1}}{dt} &= \frac{i_1}{C_1} - \frac{i_2}{C_1}\left[\frac{L_1}{v_g} i_{ref} + \frac{v_1}{v_g}\right] \\
\frac{d_{i2}}{dt} &= \frac{v_1}{L_2}\left[\frac{L_1}{v_g} i_{ref} + \frac{v_1}{v_g}\right] + \frac{v_2}{L_2} \\
\frac{d_{v2}}{dt} &= \frac{i_2}{C_2} - \frac{v_{C2}}{R_{C2}} \\
\frac{d_{v1}}{dt} &= \frac{i_{ref}}{C_1} - \frac{L_1}{C_1 v_g} i_2 i_{ref} - \frac{v_1 i_2}{C_1 v_g} = g_1(x) && (62) \\
\frac{d_{i2}}{dt} &= \frac{L_1}{L_2 v_g} v_1 i_{ref} + \frac{v_1^2}{L_2 v_g} - \frac{v_2}{L_2} = g_2(x) && (63) \\
\frac{d_{v2}}{dt} &= \frac{i_2}{C_2} - \frac{v_{C2}}{R_{C2}} = g_3(x) && (64)
\end{aligned}$$

B. IDEAL SLIDING MODE CONTROL SMC DYNAMICS

Obtaining the Jacobian of the equations we obtain the matrix:

$$J = \begin{vmatrix} \frac{\partial g_1}{\partial v_1} & \frac{\partial g_1}{\partial i_2} & \frac{\partial g_1}{\partial v_2} \\ \frac{\partial g_2}{\partial v_1} & \frac{\partial g_2}{\partial i_2} & \frac{\partial g_2}{\partial v_2} \\ \frac{\partial g_3}{\partial v_1} & \frac{\partial g_3}{\partial i_2} & \frac{\partial g_3}{\partial v_2} \end{vmatrix} X^*$$

Linearizing the system around the generic equilibrium point, we obtain:

X^* = Steady state values or an equilibrium point.

$$\begin{aligned}
&G_1(X^*) \equiv 0 \\
&\frac{I_{ref}}{C_1} - \frac{L_1}{C_1 v_g} I_2 \frac{\mathrm{d}}{\mathrm{dt}}\left(I_{ref}\right) - \frac{V_1 I_2}{C_1 v_g} = 0 \\
&\frac{I_{ref}}{C_1} = \frac{V_1 I_2}{C_1 v_g} \\
&I_{ref} = \frac{V_1^* I_2^*}{v_g} \\
&G_2(X^*) \equiv 0 \\
&\frac{L_1}{L_2} V_1^* \frac{\mathrm{d}}{\mathrm{dt}}\left(I_{ref}\right) + \frac{V_1^2}{L_2 v_g} - \frac{V_2}{L_2} = 0 \\
&\frac{V_1^{*2}}{v_g} = V_2^*
\end{aligned}$$

$$\begin{aligned}
&V_1^* = \sqrt{v_g V_2}^* && (65) \\
&G_3(X^*) \equiv 0 \\
&I_2^* = \frac{V_2^{*2}}{R} \\
&V_2^* = V_{ref} && (66)
\end{aligned}$$

$$X^* = \begin{vmatrix} I_{ref} \\ V_1^* \\ I_2^* \\ V_2^* \end{vmatrix} = \begin{vmatrix} \frac{1}{R}\sqrt{\frac{V_{ref}^3}{V_g}} \\ \sqrt{V_g V_{\mathrm{ref}}} \\ \frac{V_{\mathrm{ref}}}{R} \\ V_{\mathrm{ref}} \end{vmatrix} \tag{67}$$

$$\begin{aligned}
&\frac{\partial g_1}{\partial v_1} = -\frac{I_2}{C_1 v_g} \\
&\frac{\partial g_1}{\partial i_2} = \frac{L_1}{C_1 v_g}\frac{\mathrm{d}}{\mathrm{dt}}\left(I_{ref}\right) - \frac{V_1^*}{C_1 v_g} \\
&\frac{\partial g_1}{\partial i_2} = -\frac{V_1^*}{C_1 v_g} && (68) \\
&\frac{\partial g_1}{\partial v_2} = 0 && (69) \\
&\frac{\partial g_2}{\partial v_1} = \frac{L_1}{L_2 v_g}\frac{\mathrm{d}}{\mathrm{dt}}\left(I_{ref}\right) + \frac{2V_1^*}{L_2 v_g} = \frac{2V_1^*}{L_2 v_g} && (70) \\
&\frac{\partial g_2}{\partial i_2} = 0 && (71) \\
&\frac{\partial g_2}{\partial v_2} = -\frac{1}{L_2} && (72) \\
&\frac{\partial g_3}{\partial v_1} = 0 && (73) \\
&\frac{\partial g_3}{\partial i_2} = \frac{1}{c_2} && (74) \\
&\frac{\partial g_3}{\partial v_2} = -\frac{1}{Rc_2} && (75)
\end{aligned}$$

Now clearing, we have the partial derivatives of ∂g_1, ∂g_2, and ∂g_3 for *iref* as follows:

$$\begin{aligned}
&\frac{\partial g_1}{\partial_{iref}} = \frac{1}{c_1} && (76) \\
&\frac{\partial g_1}{\partial_{iref}} = -\frac{L_1}{c_1 v_g} I_2^* = \frac{-L_1 V_{ref}}{Rc_1 v_g} && (77) \\
&\frac{\partial g_2}{\partial_{iref}} = 0 && (78) \\
&\frac{\partial g_2}{\partial_{iref}} = \frac{L_1}{L_2}\frac{V_1^*}{V_g} = \frac{L_1}{L_2}\sqrt{\frac{V_{ref}}{V_g}} && (79) \\
&\frac{\partial g_3}{\partial_{iref}} = 0 && (80)
\end{aligned}$$

$$J = \begin{vmatrix} \frac{-I_2^*}{C_1 V_g} & \frac{-V_1^*}{C_1 V_g} & 0 \\ \frac{2V_1^*}{L_2 V_g} & 0 & \frac{-1}{L_2} \\ 0 & \frac{1}{C_2} & \frac{-1}{RC_2} \end{vmatrix} \tag{81}$$

$$J = \begin{vmatrix} \frac{-V_{ref}}{RC_1V_g} & \frac{-1}{C_1}\sqrt{\frac{V_{ref}}{V_g}} & 0 \\ \frac{2}{L_2}\sqrt{\frac{V_{ref}}{V_g}} & 0 & \frac{-1}{L_2} \\ 0 & \frac{1}{C_2} & \frac{-1}{RC_2} \end{vmatrix} \quad (82)$$

C. DYNAMIC SLIDING MODE CONTROL SMC IDEAL LINEARIZED

According to the control law, for both sides of the slip line, the corresponding substructures are directed at least in a small region towards the slip line.

$$\frac{d\tilde{v}_1}{dt} = a_{11}\tilde{v}_1 + a_{12}\tilde{i}_2 + a_{13}\tilde{v}_2 + a_{14}\tilde{i}_{ref} + a_{15}\tilde{i}_{ref} \quad (83)$$

$$\frac{d\tilde{i}_2}{dt} = a_{21}\tilde{v}_1 + a_{22}\tilde{i}_2 + a_{23}\tilde{v}_2 + a_{24}\tilde{i}_{ref} + a_{25}\tilde{i}_{ref} \quad (84)$$

$$\frac{d\tilde{v}_2}{dt} = a_{31}\tilde{v}_1 + a_{32}\tilde{i}_2 + a_{33}\tilde{v}_2 + a_{34}\tilde{i}_{ref} + a_{35}\tilde{i}_{ref} \quad (85)$$

$$\begin{vmatrix} \frac{d\tilde{v}_1}{dt} \\ \frac{d\tilde{i}_2}{dt} \\ \frac{d\tilde{v}_2}{dt} \end{vmatrix} = \begin{vmatrix} \frac{-V_{ref}}{RC_1V_g} & \frac{-1}{C_1}\sqrt{\frac{V_{ref}}{V_g}} & 0 \\ \frac{2}{L_2}\sqrt{\frac{V_{ref}}{V_g}} & 0 & \frac{-1}{L_2} \\ 0 & \frac{1}{C_2} & \frac{-1}{RC_2} \end{vmatrix} \begin{vmatrix} \tilde{v}_1 \\ \tilde{i}_2 \\ \tilde{v}_2 \end{vmatrix} + \begin{vmatrix} \frac{1}{C_1} & \frac{-L_1V_{ref}}{RC_1V_g} \\ 0 & \frac{L_1}{L_2}\sqrt{\frac{V_{ref}}{V_g}} \\ 0 & 0 \end{vmatrix} \begin{vmatrix} i_{ref} \\ i_{ref} \end{vmatrix} \quad (86)$$

Now we must deduce the transfer function of the linearized system as follows:

$$G_{vi}(s) = \frac{v_2(s)}{i_{ref}(s)} \quad (87)$$

The structure of the linear compensator is:

$$\frac{d\tilde{v}_1}{dt} = a_{11}\tilde{v}_1 + a_{12}\tilde{i}_2 + +a_{14}\tilde{i}_{ref} + a_{15}\tilde{i}_{ref} \quad (88)$$

$$\frac{d\tilde{i}_2}{dt} = a_{21}\tilde{v}_1 + +a_{23}\tilde{v}_2 + +a_{25}\tilde{i}_{ref} \quad (89)$$

$$\frac{d\tilde{v}_2}{dt} = +a_{32}\tilde{i}_2 + a_{33}\tilde{v}_2 \quad (90)$$

$$SV_1(s) = a_{11}V_1(s) + a_{12}I_2(s) + a_{14}I_{ref}(s) + a_{15}sI_{ref}(s)$$

$$SI_2(s) = a_{21}V_1(s) + a_{23}V_2(s) + a_{25}sI_{ref}(s) \quad (91)$$

$$SV_2(s) = a_{32}I_2(s) + a_{33}V_2(s) \quad (92)$$

$$(S - a_{11})V_1(s) = a_{12}I_2(s) + (a_{14} + a_{15}s)I_{ref}(s) \quad (93)$$

$$V_1(s) = \frac{a_{12}}{(s-a_{11})}I_2(s) + \frac{(a_{14}+a_{15}s)}{(s-a_{11})}I_{ref}(s) \quad (94)$$

$$sI_2(s) = \frac{a_{12}a_{21}}{(s-a_{11})}I_2(s) + a_{21}\frac{(a_{14}+a_{15}s)}{(s-a_{11})}I_{ref}(s) + a_{23}V_2(s) + a_{25}sI_{ref}(s) \quad (95)$$

$$I_2(s) = \left[\frac{a_{25}s^2 + (a_{15}a_{21} - a_{11}a_{25})s + a_{14}a_{21}}{s^2 - a_{11}s - a_{12}a_{21}}\right]I_{ref}(s) + \frac{a_{23}(s-a_{11})V_2(s)}{s^2 - a_{11}s - a_{12}a_{21}} \quad (96)$$

Proposing the desired transfer function in a closed loop, through the input-output representation of the linear compensator, results:

$$G_{v2i_{ref}}(s) = \frac{v_2(s)}{i_{ref}(s)} = \frac{\beta_2 s^2 + \beta_1 s + \beta_0}{s^3 + \propto_2 s^2 + \propto_1 s + \propto_0} \quad (97)$$

where: From the fundamental design equation:

$$\beta_2 = a_{32}a_{25} \quad (98)$$

$$\beta_1 = a_{32}(a_{15}a_{21} - a_{11}a_{25}) \quad (99)$$

$$\beta_0 = a_{32}a_{14}a_{21} \quad (100)$$

$$\propto_2 = -(a_{11} + a_{33}) \quad (101)$$

$$\propto_1 = -(a_{12}a_{21} - a_{11}a_{33} + a_{23}) \quad (102)$$

$$\propto_0 = (a_{12}a_{21}a_{33} + a_{11}a_{23}) \quad (103)$$

$$a_{11} = \frac{-V_{ref}}{RC_1V_g} \quad (104)$$

$$a_{12} = \frac{-1}{C_1}\sqrt{\frac{V_{ref}}{V_g}} \quad (105)$$

$$a_{14} = \frac{1}{C_1} \quad (106)$$

$$a_{15} = \frac{-L_1V_{ref}}{RC_1V_g} \quad (107)$$

$$a_{21} = \frac{2}{L_2}\sqrt{\frac{V_{ref}}{V_g}} \quad (108)$$

$$a_{23} = \frac{-1}{L_2} \quad (109)$$

$$a_{32} = \frac{1}{C_2} \quad (110)$$

$$a_{33} = \frac{-1}{RC_2} \quad (111)$$

With the support of the MATLAB technological tool, the simulation script is incorporated considering the construction parameters, with which the transfer function Gv2iref is obtained.

$$\text{Gv2iref} = \frac{3554s^2 - 1.496\text{e}05s + 1.974\text{e}10}{\text{s\^{}3} + 1042s^2 + 7.447\text{e}05s + 7.018\text{e}08} \quad (112)$$

To validate the transfer function, the Bode plot of the Gv2iref response in Figure 6 is verified.

Concerning the magnitude graph, it can be seen that the signal remains above 30db, and generates a slope of almost 80db per decade, in a very fast time, then a slow fall as on peak again to -10db, for the graph The phase curve is seen to be negative from 360 to -160 degrees over four decades, with a rapid drop from 10 to 3 with a small overshoot of a

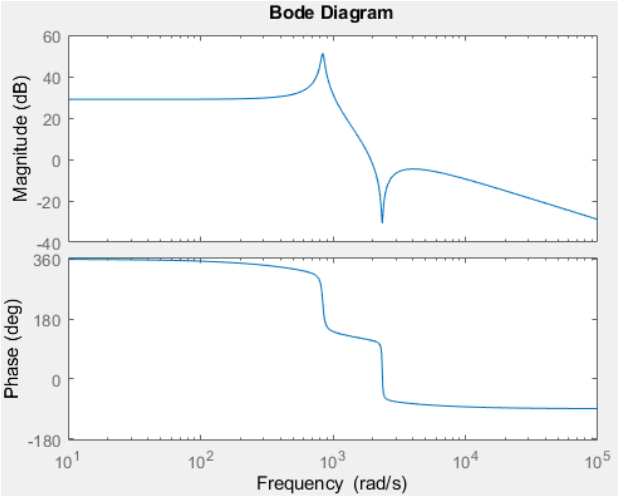

FIGURE 6. Bode plot of the control response in the sliding mode control SMC for a QBC.

central decade. To adjust the response conditions against disturbances, a PI comparator is incorporated from the transfer function.

D. CONTROLLER SLIDING MODE CONTROL SMC

The controller uses a PI (Proportional-Integral) strategy to adjust the inductor current and keep the voltage across the capacitor close to the reference value. The output of the controller is used to set the duty cycle of the converter, which in turn controls the current flowing through the inductor and capacitor. The state of the system is updated at each iteration of the loop using the system equations, which model the behavior of the inductor and the capacitor. It is important to note that a real controller must include additional safety measures, such as limits on inductor current and duty cycle, and must also consider factors such as temperature and load on the circuit.

From the sliding mode control SMC model, using MATLAB.

To design this controller, the current output concerning the reference current is considered, given by

$$S(x) = i_1(t) - i_{ref}(t)$$

Therefore, it is achieved with a PI adjustment to the reference voltage by subtracting the current output iL_1, to provide the type II compensator as explained below.

E. TYPE II COMPENSATOR

It is a circuit used to improve the frequency response of a control system in the high-frequency range. One way to implement a type II compensator using op amps is by using a circuit called a ''loop canceller'' [29].

The loop canceller is a circuit that is placed in parallel with the control loop of a control system. The loop canceller includes an operational amplifier and a feedback network that has the effect of canceling the feedback signal from the control system at high frequencies. This allows the control system to have a flatter frequency response in the high-frequency range, known as ''Type II compensation'' [30].

The loop canceller is adjusted by using an external feedback network that allows the frequency response of the control system to be adjusted in the high-frequency range. Tuning is done by using an external feedback network that allows the gain of the op-amp to be tuned in the high-frequency range [31]. It is important to note that the loop canceller is not the only type of type II compensator that can be implemented using op-amps. Other types of Type II compensators include the Polack compensator and the Ziegler-Nichols compensator, OTA (Operational Transconductance Amplifier) [32].

For the experimental case, the type II compensator was used as a circuit to improve the frequency response of a control system in the high-frequency range to improve stability and performance in the high-frequency range.

The frequency response of a control system refers to how the system behaves at different frequencies. A control system may have a flat frequency response, meaning no attenuation or gain at different frequencies, or it may have a frequency response that varies with frequency to improve the frequency response of a control system at the same time. High-frequency range, allowing the system to have a flatter frequency response in that frequency range.

There are several ways to implement a type II compensator, including the use of op-amps and other circuit design techniques. Type II compensators are often used in industrial process control systems, motor control systems, and robot control systems [33].

At a technical level, the OTA was used. An operational amplifier (Op-Amp) is a device that is used in the construction of control circuits and requires local feedback (between its output and inputs) to be stable and can be configured in many ways. different for the design of the control loop. The resistor at the bottom of the circuit (R4) does not affect the gain phase plot in Op-Amp applications, while the resistor at the top (R1) changes the gain phase. On adjustable regulators with Op-Amp, it is best to change the bottom feedback resistor while keeping the top resistor unchanged if you want to change the output voltage. Furthermore, the error amplifier may be a voltage-to-current amplification device, i.e., a transconductance operational amplifier (OTA). This is an open-loop amplifier with no local feedback. For OTA both R1 and R4 go into the AC analysis and note that only the ratio between the feedback resistors is important. The Type II compensation scheme adds an RC branch to flatten the gain and improve phase response in the midrange. Type II compensators are generally used for current mode control compensation because they cannot be used to improve power stage phasing. The Type III compensation scheme adds another RC branch to the Type II compensator and is used to compensate voltage-mode converters operating on CCM. Note that a Type III compensator with OTA does not offer the same design flexibility as a compensator with an op-amp, since the relationship between the output voltage and

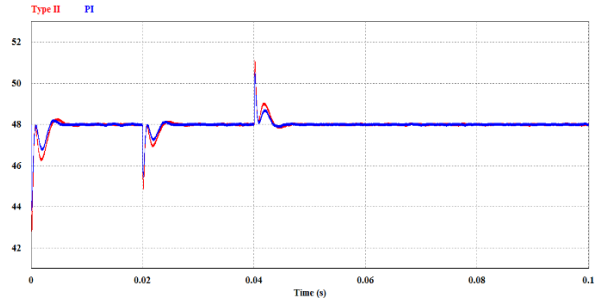

FIGURE 7. PI and voltage compensator output control.

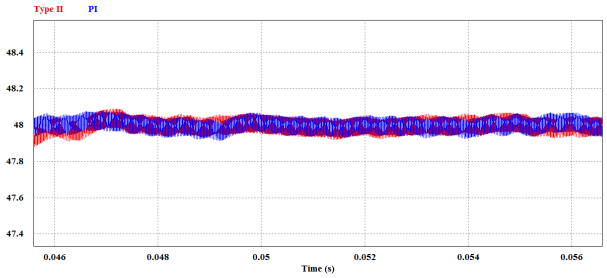

(a) Vc2 in steady state from 0.04 ms

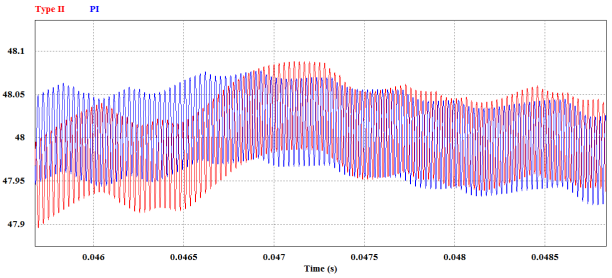

(b) Amplitude of the Vc2 PI and type II signal

FIGURE 8. Waveform PI and voltage compensator output control design, by convention PI blue type II red, PSIM.

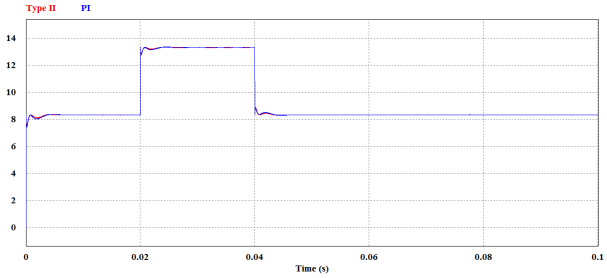

(a) Inductor current with disturbance

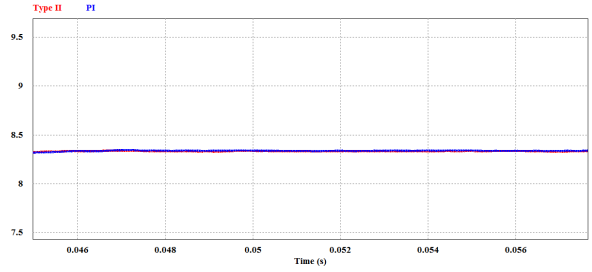

(b) steady state for current after 0.04 ms

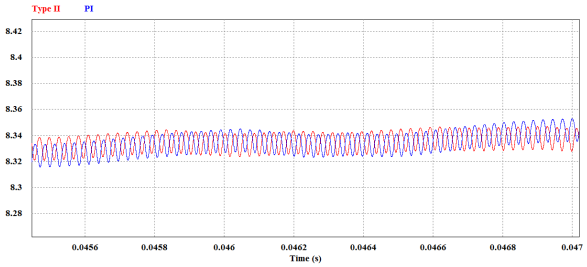

(c) Amplitude of the iL_2 PI and type II signal

FIGURE 9. Waveform PI and current compensator output control design, by convention PI blue type II red, PSIM.

the reference voltage can make it difficult to place the second zero and the first pole [34].

A compensator and pi system in sliding mode control SMC is used to control the dynamic behavior of a system. The compensator is responsible for making the system follow the desired behavior, while the pi controller is responsible for maintaining the variation of the system at a desired value.

To better understand how these systems work, it is important to note that slip mode control is based on observing the dynamic behavior of the system and using a slip function to generate a control signal that automatically adjusts to maintain the variation of the system in a desired value.

The compensator and the PI controller work together to control the dynamic behavior of the system and keep the system variation at a desired value. The compensator uses a slip function to generate a control signal that automatically adjusts to maintain system behavior on a desired trajectory. The pi controller uses an error signal to adjust the control signal generated by the compensator to maintain system variation at the 48 VDC voltage value [35].

According to the specifications and the design for the simulation of the power system, the Power Simulation PSIM tool is used, which allows modeling and simulating from distribution systems at the end consumer level to high voltage transmission and generation systems, allows the analysis of stability and control, it also evaluates the dynamic behavior of the power system [36]. design, by convention PI blue type II red, PSIM The graphs of the use of the PI control strategy and the Type II Compensator are found in Figures 7, 8, and 9 with disturbances.

The current output with disturbance from 0.02ms to 0.04ms is shown below.

Recovery after a disturbance during times of 0.04 in continuous driving mode

Finally, the validation of the compensator and PI signal in the system for the current output in the inductor

The answer is found in greater detail in MATLAB's Simulink tool.

VIII. PASSIVITY-BASED CONTROL PBC FOR DC POWER CONVERTERS

For the construction of the controller based on passivity, consider its energy modeling according to [37]. From a general

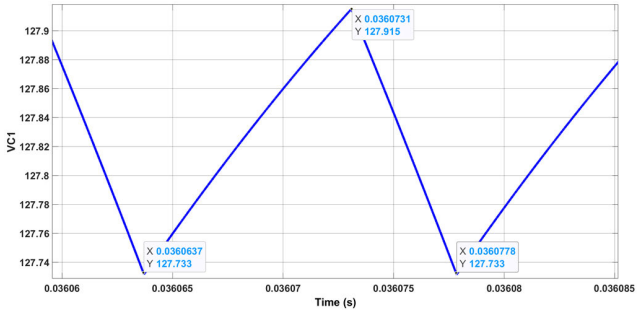

FIGURE 10. Output v_{C1} voltage ripple, from the controller in sliding mode control SMC.

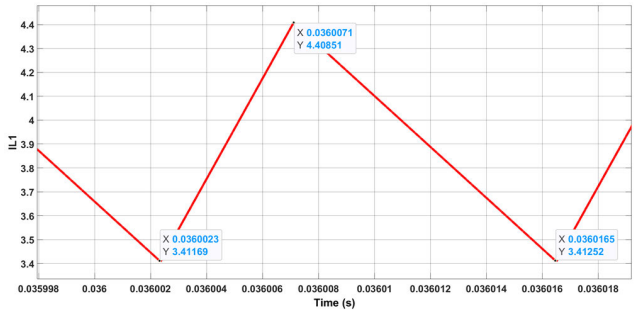

FIGURE 11. Current ripple in iL_1.

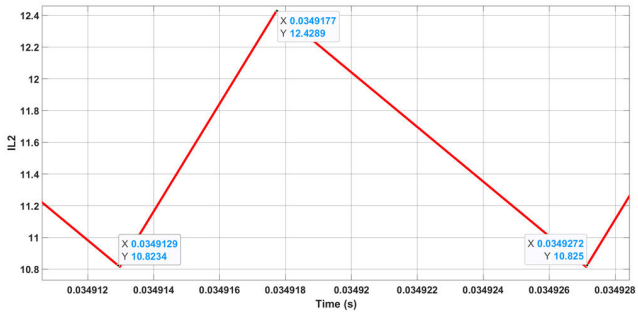

FIGURE 12. Current ripple in resistor load iL_2.

average model present in some quadratic topology direct current converters, which presents the following structure.

$$A\dot{x} = \zeta\,(u_{av})\,xRx + bu_{av} + \varepsilon \tag{113}$$

Being A is a nonnegative diagonal matrix, the symmetric matrix $\boldsymbol{\zeta}(\boldsymbol{u_{av}})$ is an array at all $\boldsymbol{u_{av}}$ with an oriented function at the input U which measures the conservative forces of the system $\boldsymbol{\zeta 0} + \boldsymbol{\zeta u}$, the nonnegative semidefinite matrix R containing the general dissipation terms of the circuit model B, also a vector with constant external forces, whose components depend on external power supplies. Finally, $\boldsymbol{\varepsilon}$ which likewise contains constant voltage values given by external sources which are measured by the vector $\boldsymbol{x\epsilon R_n}$.

Passive control follows the state path that is referenced as, $\boldsymbol{x^*(t)}$ according to the structure of the system with a candidate Lyapunov function to control the output trajectory, using the segment error $e = (x - x^*(t))$, that constitutes:

$$v\,(e) = \frac{1}{2}e^T A_e = \frac{1}{2}(x - x^*(t))A(x - x^*(t)) \tag{114}$$

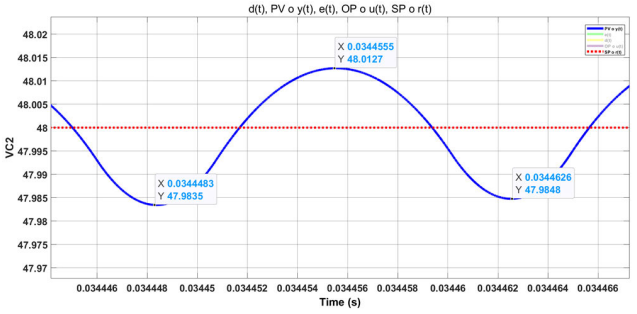

FIGURE 13. Output vc_2 voltage ripple, from the controller in sliding mode control SMC.

And its derivative for time is:

$$\begin{aligned}\dot{v}\,(e) &= (\mathrm{x} - \mathrm{x}^*(\mathrm{t}))^T \mathrm{A}(\dot{\mathrm{x}} - \dot{\mathrm{x}}^*(\mathrm{t})) \\ &= (\mathrm{x}) - \mathrm{x}^*\,(\mathrm{t})^T \left([\zeta\,(u_{av}) - R]\,x + b + \varepsilon - A\dot{x}^*\,(t)\right)\end{aligned} \tag{115}$$

Which rearranging we get:

$$A\dot{x} * (t)) = \zeta(u_{av})\mathrm{x}^*(\mathrm{t}) - R\mathrm{x}^*(\mathrm{t}) + bu_{av} + \varepsilon + RI(x - \dot{\mathrm{x}}^*(t)) \tag{116}$$

With a segmented nonnegative symmetric matrix RI that satisfies the condition given $R + RI > O$

Evaluating the dynamic trajectory $\mathrm{e}^T\zeta(\mathrm{u})\mathrm{e} = 0$, for all u, given the Lyapunov function V(e) with respect to its derivative with respect to time

$$\dot{\mathrm{V}}\,(\mathrm{e}) = \mathrm{e}^T\,(\zeta\,(u_{av})\,\mathrm{e} - \mathrm{Re} - \mathrm{R}_{Ie}) = -\mathrm{e}^T\,(\mathrm{R} + R_I)\,\mathrm{e} < 0 \tag{117}$$

where the error starts from an asymptotically stable equilibrium point, where its desired equilibrium point can have an exponential behavior.

So that its eigenvalues K_A Y $K_R + R_I$, are nonnegative and symmetric, so A y $R + R_I$ with $K = min\,\{K_A$ Y $K_R + R_I\}$, Determine its stability by:

$$\dot{\mathrm{V}}\,(\mathrm{e}) = -\mathrm{e}^T\,(\mathrm{R} + R_I)\,\mathrm{e} - \mathrm{KV}\,(\mathrm{e}) \tag{118}$$

Therefore, the RI matrix couples the stability characteristics with the damping matrix R, therefore R+RI > O is a dissipation condition since the structure of the matrix b achieves the feedback damping, therefore the spaces B are not necessarily independent R_I and B.

$$\begin{aligned}A\dot{x}^*\,(t) &= \zeta\,(u_{av})\,x^*\,(t) - Rx^*\,(t) + bu_{av} + \varepsilon \\ &+ R_I\left(x - x^*\,(t)\right)\end{aligned} \tag{119}$$

The controlled system and its additional damping:

$$R_I\left(x - x^*\,(t)\right) \tag{120}$$

complements the initial dynamics, and the error is a reference model with good dissipation, which determines an excellent trajectory for an output state with feedback, in desired minimum phase output conditions, independent of the reference dynamics, which determines the robust controller.

A. PASSIVITY-BASED CONTROL PBC

The normalized model contains a passive map of the average input $\boldsymbol{u_{av}}$ and the conductor current, in this case $\boldsymbol{x_1}$. According to the normalized averaged model, we have:

$$\begin{aligned} \dot{x}_1 &= -x_2 + u_{av} \\ \dot{x}_2 &= x_1 - u_{av}x_3 \\ \propto_1 \dot{x}_3 &= u_{av}x_2 - x_4 \\ \propto_2 \dot{x}_4 &= x_3 - \frac{1}{Q}x_4 \end{aligned} \tag{121}$$

The parameterized balance points for the output voltage are given by the constants $\boldsymbol{x_4} = \bar{\boldsymbol{x}}_{\boldsymbol{4}}$ finding what:

$$\bar{x}_1 = \frac{\sqrt{x^4}^3}{Q}; \quad \bar{x}_2 = \sqrt{\bar{x}_4}; \; \bar{x}_3 = \frac{\bar{x}_4}{Q} \tag{122}$$

The output voltage x_4 a non-minimum phase that differs from the inductor's current x_1, which is a minimum phase output. This requires that the output voltage indirectly regulates the inductor current x_1 1 approaching its equilibrium point.

The normalized average total energy stored in the converter is:

$$H\,(x) = \frac{1}{2}\left(x_1^2 + x_2^2 + \propto_1 {x_3}^2 + \propto_2 x_4^2\right) \tag{123}$$

where the derivative to time $H\,(x)$ es:

$$\dot{H}\,(x) = -\frac{1}{Q}x_4^2 + x_1 u_{av} \leq x_1 u_{av} \tag{124}$$

showing a passive map between the average control input u_{av}, and the recent, and time integral H, is known as the passive inequality, shown below:

$$H\,|x(t)| - H\,|x\,(o)| \leq \int_o^t x_1\,(\sigma)\,u_{av}\,(\sigma)\,d_\sigma \tag{125}$$

When the damping is fed back, the auxiliary system is added, utilizing $R_1\,(x_1 - x_{1d})\,, R_1 > o$ Therefore,

$$\begin{aligned} \dot{x}_{1d} &= -x_{2d} + u_{av} + R_1(x_1 - x_{1d}) \\ \dot{x}_{2d} &= x_{1d} - u_{av}x_{3d} \\ \propto_1 \dot{x}_{3d} &= u_{av}x_{2d} - x_{4d} \\ \propto_2 \dot{x}_{4d} &= x_{3d} - \frac{x_{4d}}{Q} \end{aligned} \tag{126}$$

Considering the average normalized error variables

$$e_i = x_i - x_{id}, \quad i = 1, \ldots, 4.$$

The dynamics of the error are given by:

$$\begin{aligned} \dot{e}_1 &= -e_2 - R_1 e_1 \\ \dot{e}_2 &= e_1 - u_{av}e_3 \\ \propto_1 \dot{e}_3 &= u_{av}e_2 - e_4 \\ \propto_2 \dot{e}_4 &= e_3 - \frac{1}{Q}e_4 \end{aligned} \tag{127}$$

TABLE 1. QBC Found parameter values.

L_1	L_2	C_1	C_2	R	E
$1{,}2mH$	$250\mu H$	$200\mu f$	$100\mu f$	4.7Ω	$380v$

Regarding the Lyapunov function, taken from the error space obtained in the tracking of the trajectory given by the coordinates, $e = (e_1, e_2, e_3, e_4)$, you must:

$$H\,(e) = \frac{1}{2}(e_1^2 + e_2^2 + \propto_1 e_3^2 + \propto_2 e_4^2) \tag{128}$$

The derivative of the previous non-negative function, where the trajectory control produces an error dynamic given by:

$$\dot{H}\,(e) = -R_1 e_1^2 - \frac{1}{Q}e_4^2 \leq 0 \tag{129}$$

Satisfying the fit points in the error space from $\dot{H}(e) = 0$, by crossing the hyperplanes, $e_1 = e_4 = 0$ thus $e_3 = 0$ and $e_2 = 0$, according to Lasalle's theorem, and the equilibrium point $e_i = 0, i = 1 \ldots .4$, whose equilibrium point is globally asymptotically stable, therefore the approximate trajectory system, $x(t)$, as well as the auxiliary trajectories $x_d\,(t)$, both converge asymptotically; obtaining the exact value of equilibrium in the desired average inductor current X_{1d} for the dynamics of the auxiliary system, the control input Uav of the auxiliary dynamics equation for the dynamic average feedback controller Uav is given by:

$$\begin{aligned} u_{av} &= \xi_2 - R_1(x_1 - \overline{x_1}) \\ \xi_2 &= \overline{x_1} - u_{av}\xi_3 \\ \propto_1 \xi_3 &= u_{av}\xi_2 - \xi_4 \\ \propto_2 \xi_4 &= \xi_3 - \frac{1}{Q}\xi_4 \end{aligned} \tag{130}$$

Variables $\xi_2, \xi_3\, y\, \xi_4$ are part of the dynamic state controller, and finally by incorporating the auxiliary state variables x_{2d}, x_{3d} *and* x_{4d} that is going to be replaced in the auxiliary dynamic model, we must:

$$x_{1d} = \overline{x_1} \tag{131}$$

The input signal u_{av} is the approximate dynamic closed-loop derivative of the controller and is represented by the normalized approximation of input or lead current x_1, for the dynamic closed-loop output of the controller.

The modulator $A\Sigma - \Delta$. It is used in the implementation of the u_{av} input for the switched model applied to the approximate closed-loop control law.

B. VALUES FOUND IN THE SIMULATIONS

Given a converter that is parameterized as follows:

That normalized values can be achieved.

$$Q = R\sqrt{\frac{C}{L}}, \quad Q_{L1} = 40.9480x10^{-3}, \; Q_{L2} = 1.29489$$

$\alpha_1 = 1, \alpha_2 = 1$, for the desired voltage $\overline{v_2} = 48v = Vd$

With steady-state values for the other missing state variables: $\overline{i_1} = 3,7022A$, $\overline{v_1} = 135.05v$, $\overline{i_2} = 10,4167A$, $\overline{U_{av}} = \sqrt{48}$.

By implementing the closed-loop passivity-based stabilization Σ-Δ modular that obeys the mean passivity controller, which represents its mean square response of the System through the actions, designed from the model based on the energy and the actions perturbed by the system damping.

C. ACCURATE ERROR DYNAMICS PASSIVE OUTPUT FEEDBACK CONTROL

The exact dynamic model of the stabilization error of the average system model, according to the management structure due to the error dynamics in terms of energy in orientation to the generalized Hamiltonian form, and its response for this case is passive for the dynamics of stabilization error.

Its main characteristic is based on generating simple linear feedback, with time invariance, which converts an asymptotic and globally stable point into a closed loop, structurally dissipated for its adaptation to the system.

D. RESULTS OBTAINED

The general normalized model of the DC-DC QBC, written in a generalized Hamiltonian canonical way it can be expressed as:

$$\ddot{x} = \zeta\,(u_{av})\,\frac{\partial H}{\partial x} - R\frac{\partial H}{\partial e} + bu_{av} + \varepsilon \tag{132}$$

Since $\mathscr{H}(\boldsymbol{x})$ is the energy present in the system, described as $\mathscr{H}(\mathrm{X}) = \frac{1}{2}\boldsymbol{x}^{\boldsymbol{T}}\boldsymbol{x}$ where $\partial^{\mathscr{H}}/\partial_{\mathrm{x}} = \boldsymbol{x}$ being the matrix $\boldsymbol{\zeta}\,(\boldsymbol{u_{av}})$ oblique, R is a semidefinite non-negative symmetric matrix, and finally, the vector $\boldsymbol{b}$ is the constitutive constant and ε given by the external supply to the system.

Therefore, the generalized Hamiltonian form is the fit of the normalized form of the converter, as shown below:

$$\zeta\,(u_{av}) = \begin{bmatrix} 0 & -1 & 0 & 0 \\ 1 & 0 & -u_{av} & 0 \\ 0 & u_{av} & 0 & -1 \\ 0 & 0 & 1 & 0 \end{bmatrix}, \quad b = \begin{bmatrix} 1 \\ 0 \\ 0 \\ 0 \end{bmatrix}, \varepsilon = 0 \tag{133}$$

For a linear converter the matrix $\boldsymbol{\zeta}\,(\boldsymbol{Uav}) = \boldsymbol{\zeta}$ is constant.

However, for the nonlinear QBC $\boldsymbol{\zeta}\,(\boldsymbol{Uav})$, the matrix is biased symmetrically, to the average control input $\boldsymbol{Uav}$, it can be said that $\boldsymbol{\zeta}\,(\boldsymbol{Uav})$ satisfies its constant *values* $\overline{\overline{\boldsymbol{U}}}$, and by applying the expansion property.

$$\zeta\,(u_{av}) = \zeta\,(\overline{u}) + \left.\frac{\partial \zeta\,(u_{av})}{\partial u_{av}}\right|_{u_{av}=\overline{U}} (u_{av} - \overline{u}) \tag{134}$$

As defined $\boldsymbol{\zeta}\,(\boldsymbol{u_{av}})$ implies $\boldsymbol{u_{av}}$, the matrix $\frac{\partial \zeta(u_{av})}{\partial u_{av}}$ is constant and with biased symmetrical characteristics.

Therefore, in the equilibrium point equations, it behaves as follows:

$$0 = \zeta\,(g)\,\frac{\partial H}{\partial x}|_{x=x} - R\frac{\partial H}{\partial x}|_{x=x} + bu + \varepsilon \tag{135}$$

$$0 = \zeta\,(u)\,x - Rx + bu + \varepsilon \tag{136}$$

Given $\overline{x}$ as a steady state approximation constant, with the output control average constant $\overline{u}$ satisfying $\overline{u} \in [0, 1]$. Therefore, when applying the stabilization errors, we have

$$e = x - \overline{\mathrm{x}},\ \mathrm{e_u} = \mathrm{u_{av}} - \overline{\mathrm{u}}$$

Then,

$$e = x - \overline{x} = \frac{\partial H\,(x)}{\partial x} - \frac{\partial H(\overline{x})}{\partial(\overline{x})} = \frac{\partial H(e)}{\partial e} \tag{137}$$

Thus,

$$\dot{e} = \dot{\mathscr{X}}$$

Then we have that the stabilization error dynamics satisfy in a general way:

$$\dot{e} = \zeta\,(u_{av})\,\frac{\partial H(e)}{\partial e} - R\frac{\partial H\,(e)}{\partial e} + be_u + [\frac{\partial \zeta\,(u_{av})}{\partial u_{av}}\frac{\partial H\,(x)}{\partial x}|_{x=\overline{\mathrm{x}}}]e_u$$

So,

$$\dot{e} = \zeta\,(u_{av})\,e - R\dot{e} + [b + \frac{\partial \zeta(u_{av})}{\partial u_{av}}\overline{\mathrm{x}}]e_u \tag{138}$$

Applying the differential in the equation, we have:

$$\dot{e} = \zeta\,(u_{av})\,\frac{\partial H\,(e)}{\partial e} - R\frac{\partial H\,(e)}{\partial e} + be_u + \varepsilon + \zeta\,(u_{av})\,\frac{\partial H}{\partial x}|_{x=\overline{\mathrm{x}}} - R\frac{\partial H}{\partial x}|_{x=\overline{\mathrm{x}}} + b\overline{\mathrm{u}} \tag{139}$$

Using the equilibrium relations, we have:

$$0 = \varepsilon + \zeta\,(\overline{\mathrm{u}})\,\frac{\partial H\,(e)}{\partial x}|_{x=\overline{\mathrm{x}}} - R\frac{\partial H}{\partial x}|_{x=\overline{\mathrm{x}}} + b\overline{\mathrm{u}} \tag{140}$$

Therefore, it satisfies:

$$\dot{e} = \zeta\,(u_{av})\,\frac{\partial H(e)}{\partial e} - R\frac{\partial H\,(e)}{\partial e} + be_u + [\zeta\,(u_{av}) - \zeta\,(\overline{u})]\,\frac{\partial H}{\partial x}|_{x=\overline{\mathrm{x}}} \tag{141}$$

Given

$$\boldsymbol{\dot{e} = \zeta\,(u_{av})\,e - Re + be_u\frac{\partial \zeta\,(u_{av})}{\partial u_{av}}\overline{x}\left[\frac{\partial H}{\partial x}|_{x=\overline{x}}\right]e_u} \tag{142}$$

Then,

$$\boldsymbol{\dot{e} = \zeta\,(u_{av})\,e - Re + be_u + \frac{\partial \zeta\,(u_{av})}{\partial u_{av}}\overline{x}e_u} \tag{143}$$

Rewriting,

$$\boldsymbol{\dot{e} = \zeta\,(u_{av})\,e - Re + [b + \frac{\partial \zeta\,(u_{av})}{\partial u_{av}}\overline{x}]e_u} \tag{144}$$

To stabilize the dynamic error, it must be considered:

By definition $\boldsymbol{\zeta}\,(\boldsymbol{u_{av}})\,\boldsymbol{e} = \boldsymbol{\zeta}\,(\boldsymbol{u_{av}})\,\frac{\partial \boldsymbol{H}(\boldsymbol{e})}{\partial \boldsymbol{e}}$ is the conservative nonlinear term, to $\boldsymbol{u_{av}}$ the following definition is related:

The definition given below is related:

$$\boldsymbol{e}^{\boldsymbol{T}}\boldsymbol{\zeta}\,(\boldsymbol{u_{av}})\,\boldsymbol{e} = \frac{\partial \boldsymbol{H}(\boldsymbol{e})}{\partial \boldsymbol{e}^{\boldsymbol{T}}}\boldsymbol{\zeta}\,(\boldsymbol{u_{av}})\,\frac{\partial \boldsymbol{H}(\boldsymbol{e})}{\partial \boldsymbol{e}} = \boldsymbol{0} \tag{145}$$

which is not relevant to the stability of the input closed-loop system $\boldsymbol{e_u} = \boldsymbol{u} - \overline{\boldsymbol{u}}$

In such a way that $-\boldsymbol{Re} + \boldsymbol{be_u} + \frac{\partial \boldsymbol{\zeta}(\boldsymbol{u_{av}})}{\partial \boldsymbol{u_{av}}}\overline{\boldsymbol{x}}\boldsymbol{e_u}$, is the complement of the dynamic error, which contains the tangent linearization with the dynamic non-linearization of the matrix. $\boldsymbol{\zeta}(Uav)$ then, $\dot{\boldsymbol{x}} = \boldsymbol{\zeta}\,(\boldsymbol{u_{av}})\,\frac{\partial \boldsymbol{H}}{\partial \boldsymbol{x}} - \boldsymbol{R}\,\frac{\partial \boldsymbol{H}}{\partial \boldsymbol{x}} + \boldsymbol{bu_{av}} + \boldsymbol{\varepsilon}$

Around breakeven $x = \overline{\mathrm{x}}$, $u_{av} = \overline{u}$ in which:

$$\dot{x}\delta = \zeta\,(\overline{u})\,x\delta - Rx\delta + bu\delta + \frac{\zeta\,(u_{av})}{\partial u_{av}}\overline{x}u\delta x\delta = x - \overline{\mathrm{x}} \tag{146}$$

Considering the three terms that handle the dynamics of the error, on the side of the right half plane that generates the dynamics of the error for the stabilization of the system and its equivalence $\boldsymbol{x\delta} = \boldsymbol{x} - \overline{\boldsymbol{x}}$ with e and $\boldsymbol{u\delta} = \boldsymbol{u_{av}} - \overline{\boldsymbol{u}}$ with the use of $\boldsymbol{e_u}$.

Considering the Theorem that defines linear incremental feedback, for the controller design deduced based on zero stabilization, with the average tangent stabilization model of the system for a desired equilibrium point with a given initial condition, where for This, the average linear incremental feedback given control law:

linearized feedback model, retrieved from the tangent linearized model, defines the nonlinear equilibrium point as semi-globally or osmotically stable.

$$e_u = u_\delta = -k^T e = -k^T x_\delta \tag{147}$$

To search for stabilization, the poles of the tangent linearization averaging dynamics are demonstrated by the following: Let k_T then be a row vector of gains that feedback on the stabilization errors of the state [38]. The dynamics of the system error are expressed as:

$$\dot{e} = \zeta\,(u_{av})\,e - Re - [b + \frac{\partial \zeta\,(u_{av})}{\partial u_{av}}\overline{x}]k^T e \tag{148}$$

$$\dot{e} = \zeta\,(u_{av})\,e - [R + \left(b\frac{\partial \zeta\,(u_{av})}{\partial u_{av}}\overline{x}\right)k^T]e \tag{149}$$

Then,

$$M = [R + \left(b + \frac{\partial \zeta\,(u_{av})}{\partial u_{av}}\overline{x}\right)k^T]e \tag{150}$$

where the matrix M contains its eigenvalues on the right side of the complex plane, however, M is neither symmetric nor skew-symmetric, therefore.

$$M = \zeta M + RM \tag{151}$$

Which contains asymmetric ζM and Rm is symmetric, therefore $-Rm$ is defined as negative.

$$M = \frac{1}{2}\left[M - M^T\right] + \frac{1}{2}[M + M^T] \tag{152}$$

From there we obtain the closed loop of the system:

$$\dot{e} = [\zeta\,(Uav) - \zeta M]\,e - [R + RM]\,e \tag{153}$$

The semi-global stability of the closed-loop system is achieved from the bias symmetry of the matrix $\zeta\,(u_{av}) - \zeta M$ for u_{av}, as well as the symmetric matrix $R + R\mathrm{M}$, by the theorem defined above the stability of averaged converters is not linear this linear feedback which in turn semi-globally stabilizes the nonlinear average conversion models. which implements the closed-loop use of the positive incremental output.

Considering the standard model.

$$\begin{aligned} \dot{x_1} &= -x^2 + Uav \\ \dot{x_2} &= x_1 - Uav\,x_3 \\ \propto_1 \dot{x_3} &= Uav\,x_2 - x_4 \\ \propto_2 \dot{x_4} &= x_3 - \frac{1}{Q}x_4 \end{aligned} \tag{154}$$

Bringing the paths to a steady average state equilibrium point to obtain the equilibrium point to voltage as the desired output.

$$\overline{x_4} = V_d,\ \text{by}\ \overline{x_1} = \frac{(vd)^{3/2}}{Q},\ \overline{x_2} = \sqrt{vd},\ \overline{x_3} = \frac{vd}{Q},\ Uav = \sqrt{vd}$$

Defining from the state coordinates to the stabilization error space, it is found that:

$$\begin{aligned} e_1 &= x_1 - \frac{(vd)^{3/2}}{Q}, \quad e_2 = x_2 - \sqrt{vd}, \\ e_3 &= x_3 - \frac{vd}{Q}, \quad e_4 = x_4 - vd \end{aligned}$$

What determines the relationship:

$$\begin{aligned} \dot{e_1} &= -e_2 + (Uav - \sqrt{vd}) \\ \dot{e_2} &= e_1 - Uave_3 - \frac{vd}{Q}(Uav - \sqrt{vd}) \\ \propto_1 \dot{e_3} &= Uave_2 - e_4 + \sqrt{vd}(Uav - \sqrt{vd}) \\ \propto_1 \dot{e_4} &= e_3 - \frac{1}{Q}e_4 \end{aligned} \tag{155}$$

From the energy function to the error:

$$H\,(e) = \frac{1}{2}e^t Ae = \frac{1}{2}\left[e_1^2 + e_2^2 + \alpha_1 e_3^2 + \alpha_2 e_4^2\right]$$

where the transpose of the matrix is:

$$A = A^T = diag(1, 1, \alpha_1, \alpha_2),\ e = \left[e_1, e_2, e_3, e_4\right]^T$$

It must

$$\frac{\partial \mathrm{H(e)}}{\partial \mathrm{e}} = \mathrm{Ae} = \left[\mathrm{e_1, e_2, x_1, e_3, x_2, e_4}\right]^{\mathrm{T}} \tag{156}$$

In generalized Hamiltonian form, using the closed loop, the error stabilization system is calculated.

$$e^{\cdot} = \begin{bmatrix} 0 & -1 & 0 & 0 \\ 1 & 0 & -\frac{1}{\alpha_1}Uav & 0 \\ 0 & \frac{1}{\alpha_1}Uav & 0 & -\frac{1}{\alpha_1\alpha_2} \\ 0 & 0 & \frac{1}{\alpha_1\alpha_2} & 0 \end{bmatrix} \frac{\partial H(e)}{\partial e} - \begin{bmatrix} 0 & 0 & 0 & 0 \\ 0 & 0 & 0 & 0 \\ 0 & 0 & 0 & 0 \\ 0 & 0 & 0 & \frac{1}{\alpha_2^2 Q} \end{bmatrix} \frac{\partial H(e)}{\partial e} + \begin{bmatrix} 1 \\ -\frac{\sqrt{d}}{Q} \\ \frac{\sqrt{vd}}{\alpha_1} \\ 0 \end{bmatrix} e\ Uav \tag{157}$$

where, e_{Uav} be expressed as follows:

$$e_{Uav} = Uav - \sqrt{ud} \tag{158}$$

The presentation of the error stabilization employing the Hamiltonian method, as part of the passive output, is formed by:

$$e_y = \frac{bT\partial H(e)}{\partial e} = e_1 - \frac{vd}{Q}e_2 + \sqrt{vd}e_3 \tag{159}$$

However, it is possible to verify the adaptation of dispersion, which in this case is not completely fulfilled, because:

$$\begin{aligned} \dot{H}(e) &= -\frac{\partial H(e)}{\partial eT}[R + \gamma bbT]\frac{\partial H(e)}{de} \\ &= \left[-e^T A\left[R + \gamma, bb^T\right]\right] Ae, \leq 0 \end{aligned} \tag{160}$$

Therefore:

$$A\left[R + \Upsilon bb^T\right]A = \begin{bmatrix} \Upsilon & -\gamma\frac{vd}{Q} & \gamma\sqrt{vd} & 0 \\ -\gamma\frac{vd}{Q} & \gamma\frac{v^2d}{Q^2} & -\gamma\frac{(vd)^{\frac{3}{2}}}{Q} & 0 \\ \gamma\sqrt{vd} & -\gamma\frac{(vd)^{\frac{3}{2}}}{Q} & \Upsilon vd & 0 \\ 0 & 0 & 0 & \frac{1}{Q} \end{bmatrix} \geq 0 \tag{161}$$

It can be said that the neighborhood of these vectors is the null space of the previous matrix, given that:

$$z = [\boldsymbol{e_1\ e_2\ e_3\ 0}]$$

such that,

$$\boldsymbol{\xi\delta = e_1 - \frac{vd}{Q}e_2 + \sqrt{vd}e_3 = 0} \tag{162}$$

Contained in a subspace of $\boldsymbol{R^4}$ understood by $\boldsymbol{ey = \xi\delta}$ Therefore, in subspace, this nonlinear system is controlled by the equilibrium input $\boldsymbol{Uav = \sqrt{vd}}$, and the error is controlled by $\boldsymbol{e_{Uav} = 0}$ with a trivial error system path $\boldsymbol{e_y = 0}$ and $\boldsymbol{e_{Uav} = 0}$

Therefore, considering Lasalle's asymmetric stability theorem, for the closed loop mean error system to have an astronomically stable equilibrium as its origin, with a set of trajectories given by the origin $|\boldsymbol{e}|\ \{\dot{\boldsymbol{H}}(\boldsymbol{e}) = \boldsymbol{0}\}$

with the feedback-controlled average error system, determining an astronomically stable equilibrium.

For this, the feedback controller is given by:

$$e_{Uav} = -\gamma ey = -\gamma\left[e_1 - \frac{vd}{Q}e_2 + \sqrt{vd}e_3\right] \tag{163}$$

Therefore, the average stabilization feedback control, passive output is:

$$\begin{aligned} Uav = \sqrt{vd} - \Upsilon\Bigg[\left(x_1 - \frac{(vd)^{\frac{3}{2}}}{Q}\right) - \frac{vd}{Q}\left(x_2 - \sqrt{vd}\right) \\ +\sqrt{vd}\left(x_3 - \frac{vd}{Q}\right)\Bigg] \end{aligned} \tag{164}$$

The output feedback is incrementally passive, and the controller's initial feedback is tangent [38].

The switched stabilization response, from a feedback controller using linear static passivity.

Considering the parameters found for the quadratic Buck switch:

$$\begin{aligned} &L_1 = 1,2\ mH \quad C_1 = 200Mf\ L_2 = 250\mu H \\ &C_2 = 100Mf \\ &\boldsymbol{R = 4.7\Omega\ \ E = 380\ V} \end{aligned}$$

Choosing $\boldsymbol{\gamma = 1}$, a reference voltage $\boldsymbol{V2 = 48}\,v$

each of the real steady-state variables is determined:

$$\begin{aligned} &i_1 = 3,7022A \quad V_1 = 135,05V\ i_2 = 10,4167A \\ &\Upsilon\ Uav => \sqrt{vd} = \sqrt{48}. \end{aligned}$$

The most important outputs of the switched system, starting from the static controller based on linear passivity as a product in the passive output of the exact dynamics of the stabilization error.

IX. QUADRATIC BUCK CONTROLLER DESIGN USING CANONICAL FORMS

From the state feedback, through the methodology in controllable and observable Canonical form.

The closed-loop behavior yields the normalized nonlinear dynamics based on differential algebra, whose output for the normalized current and voltage values [39].

A. CONTROLLER DESIGN

The variable x is the normalized output current, for the voltage output corresponding to the output capacitor relative to the respective coil current.

Returning to the normalized model:

$$\begin{aligned} \dot{x_1} &= -x_2 + Uav \\ \dot{x_2} &= x_1 - Uav\ x_3 \\ \propto_1 \dot{x_3} &= Uav\ x_2 - x_4 \end{aligned}$$

$$\propto_2 \dot{x_4} = x_3 - \frac{x_4}{Q}$$
$$y = x_1 \tag{165}$$

Being one of the output degrees of the entire system, with the invertible input the dependent state coordinate transformation is performed.

$$\begin{bmatrix} z_1 \\ z_2 \\ z_3 \\ z_4 \end{bmatrix}$$
$$= \emptyset(x) = \begin{bmatrix} h_{(x)} \\ \dot{h}_{(x)} \\ \ddot{h}_{(x)} \\ h^{(3)}_{(x)} \end{bmatrix}$$
$$= \begin{bmatrix} x_1 \\ Uav - x_2 \\ \dot{U}av - Uavx_3 - x_1 \\ \ddot{U}av + x_3\dot{U}av + \frac{1}{a1}\left(Uavx_2 - x_4 - \propto_1\right) Uav + x_2 \end{bmatrix} \tag{166}$$

Which for that matter is the inverse transformation

$$\begin{bmatrix} \boldsymbol{x_1} \\ \boldsymbol{x_2} \\ \boldsymbol{x_3} \\ \boldsymbol{x_4} \end{bmatrix} = \emptyset^{-1}(\mathbf{Z}) \tag{167}$$

Therefore, the dynamics around a desired average reference balance value for the output are:

$$Uav^{(3)} + \left(\frac{\overline{z_1}}{Uav} - \frac{3}{Uav}Uav + \frac{1}{\propto_2 Q}\right)\ddot{U}av + \frac{2}{U^2av}\dot{u}^3_{av} - \left(\frac{2\overline{z}_1}{U^2_{av}} + \frac{1}{\propto_2 UavQ}\right) + \left(2\frac{U^2_{av}}{\propto_1} + \frac{1}{a_1 \propto_2} + \frac{\overline{z}_1}{\propto_2 UavQ}\right)\dot{Uav} + \frac{1}{\propto_1 \propto_2}\left(\frac{u^3av}{Q} - \overline{z_1}\right) = 0 \tag{168}$$

The roots of the polynomials determine the equilibrium points of the zero dynamics.

$$P(Uav) = \frac{1}{\propto_1 \propto_2}\left(\frac{u^3av}{Q} - \overline{z_1}\right) \tag{169}$$

Such that the given equilibrium points are:

$$Uav = \sqrt{3}Q\overline{z_1},\ Uav = \frac{1}{2}\sqrt{3}Q\overline{z_1}(1 \pm \sqrt{3}\mathrm{i}) \tag{170}$$

where $Uav = \sqrt{3}Q\overline{z_1}$ presents a different unconventional phase diagram, resorting to working it through the Lyapunov function, which determines that it is also asymptotically stable in its zero dynamics.

B. CLOSED LOOP CONTROLLER DESIGN

According to the model it is defined as:

$$\dot{z_1} = z_2;\ \dot{z_2} = z_3;\ \dot{z_3} = z_4;\ y = z_1$$
$$\dot{z_4} = Uav^3 + x_3\ddot{u}av + \frac{3Uavx_2 - 2x_4 - \propto_1}{\propto_1}\dot{U}av + \frac{\left(U^2av + \propto_1\right)(x_1 - Uavx_3)}{\propto_1} + \frac{x_4 - Qx_3}{\propto_1 \propto_2 Q}Ua \tag{171}$$

The inverse transform generates the vector of states that is constituted by (x_1, x_2, x_3, x_4)

$\dot{z_4}$ is calculated as the average closed-loop dynamic linearization given by Uav

$$\dot{z_1} = z_2;\ \dot{z_2} = z_3;\ \dot{z_3} = z_4;\ \dot{z_4} = Uav;\ y = z_1 \tag{172}$$
$$Uav = Uav^3 + x_3\ddot{u}av + \frac{3Uavx_2 - 2x_4 - \propto_1}{\propto_1}\dot{U}av + \frac{\left(U^2av + \propto_1\right)(x_1 - Uavx_3)}{\propto_1} + \frac{x_4 - Qx_3}{\propto_1 \propto_2 Q}Uav \tag{173}$$

Obtaining the balance points in $\overline{z} = (\overline{z_1}, 0, 0, 0)$

Converging the trajectories to the equilibrium point z, Uav can be defined as:

$$Uav = -B_4Z_4 - B_3Z_3 - B_2Z_2 - B_1\left(Z_1 - \overline{Z_1}\right) \tag{174}$$

Therefore, the closed-loop averaged system is:

$$\begin{bmatrix} \dot{z}_1 \\ \dot{z}_2 \\ \dot{z}_3 \\ \dot{z}_4 \end{bmatrix} = \begin{bmatrix} 0 & 1 & 0 & 0 \\ 0 & 0 & 1 & 0 \\ 0 & 0 & 0 & 1 \\ -\beta_1 & -\beta_2 & -\beta_3 & -\beta_4 \end{bmatrix} = \begin{bmatrix} z_1 - \overline{z_1} \\ z_2 - \overline{z_2} \\ z_3 - \overline{z_3} \\ z_4 - \overline{z_4} \end{bmatrix} \tag{175}$$

Therefore, the polynomial that characterizes the system is given by:

$$P(s) = S4 + \beta_4 S^3 + \beta_3 S^2 + \beta_2 S + \beta_1 \tag{176}$$

Using Ruth Hurwitz's method, a desired polynomial pd(s) is achieved. Therefore, calculating their coefficients Pd(s). Which is chosen from the determination of the stability roots, according to the observation and characterization of the behavior of the variables in the complex left half plane.

$$Pd(s) = \left(s^2 + 2\xi_1 wn_1 s + w^2 n_1\right)\left(s^2 + 2\xi_2 wn_2 s + w^2 n_2\right) = s^4 + 2\left(\xi_1 wn_1 + \xi_2 wn_2\right)s^3 + \left(w^2 n_1 + 4\xi_1\xi_2 wn_1 wn_2 + w^2 n_2\right)s^2 + 2\left(\xi_1 wn_1 w^2 n_2 + \xi_2 w^2 n_1 wn_2\right)s + w^2 n_1 w^2 n_2 \tag{177}$$

The closed-loop gains of the system are calculated by equating the coefficients of the polynomial.

$$\beta_1,\ \beta_2,\ \beta_3,\ \beta_4.$$
$$\beta_1 = w^2 n_1 w^2 n_2$$

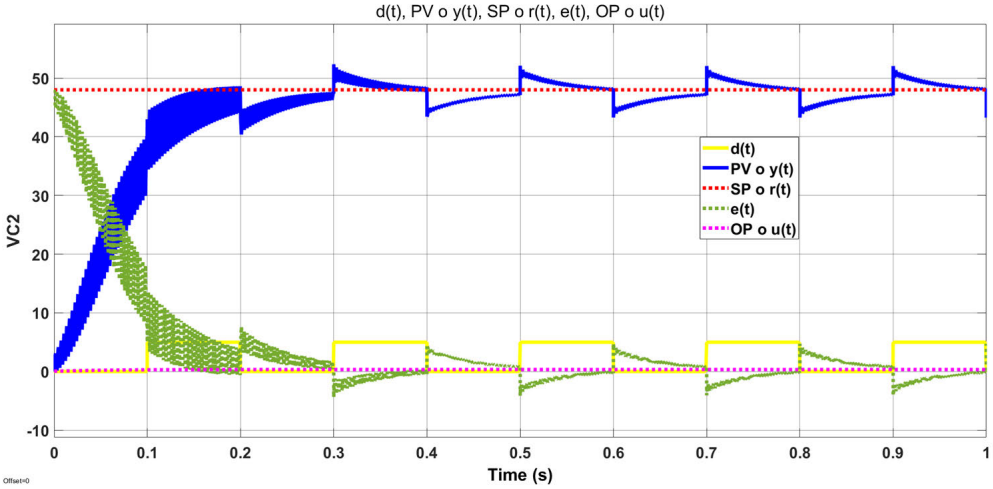

FIGURE 14. Response output V_{C2} and its validation through the disturbance and its control components.

$$\begin{aligned}\beta_2 &= 2(\xi_1 wn_1 w^2 n_2 + \xi_2 w^2 n_1 wn_2)\\ \beta_3 &= (wn_1^2 + 4\xi_1\xi_2 wn_1 wn_2 + w^2 n_2)\\ \beta_4 &= 2(\xi_1 wn_1 + \xi_2 wn_2)\end{aligned} \tag{178}$$

Equalizing, the stabilization of the system is obtained by:

$$\begin{aligned}Uav^{(3)} = &-\beta_4 Z_4 - \beta_3 Z_3 - \beta_2 Z_2 - \beta_1\left(Z_1 - \overline{Z_1}\right)\\ &- X_3 \ddot{U}av - \frac{3UavX_2 - 2X_4 - \propto_1}{\propto_1}\dot{U}av\\ &- \frac{\left(u^2 av + \propto_1\right)(\propto_1 - UavX_3)}{\propto_1} - \frac{X_4 - QX_3}{\propto_1 \propto_2 Q}Uav\end{aligned} \tag{179}$$

the state variables present in the simulations are:

$$\mu_1 = Uav, \mu_2 = \dot{U}av, \mu_3 = \ddot{U}av \tag{180}$$

Expressing the controller through these state variables we get:

$$\begin{aligned}\dot{\mu_1} &= \mu_2\\ \dot{\mu_2} &= \mu_3\\ \dot{\mu_3} &= -\beta_4 Z_4 - \beta_3 Z_3 - \beta_2 Z_2 - \beta_1\left(Z_1 - \overline{Z_1}\right) - X_3\mu_3\\ &\quad - \frac{3\mu_1 X_2 - 2X_4 - \propto_1}{\propto_1}\mu_2 - \frac{\left(\mu_1^2 + \propto_1\right)(X_1 - \mu_1 X_3)}{\propto_1}\\ &\quad - \frac{X_4 - QX_3}{\propto_1 \propto_2 Q}\mu_1\end{aligned} \tag{181}$$

Substituting

$$\begin{aligned}&Z_1, Z_2, Z_3 y Z_4\\ &Z_1 = x\\ &Z_2 = \mu_1 - X_2\\ &Z_3 = \mu_2 + \mu_1 X_3 - X_1\\ &Z_4 = \mu_3 + \mu_2 X_3 - \frac{1}{X_1}\left(\mu_1 X_2 - X_4 - \propto_1\right)\mu_1 + X_2\end{aligned} \tag{182}$$

Simulations Results: It is implemented using the $\Sigma - \Delta$ modulator according to the simulation made by MATLAB.

TABLE 2. QBC calculated parameter values.

$\overline{i_1}$	$\overline{i_2}$	$\overline{v_1}$	$\overline{v_2}$	$\overline{X_4}$	$\overline{U_{av}}$
$3{,}7022A$	$10{,}4167A$	$135.05v$	$48v$	0,25	$\sqrt{48}$

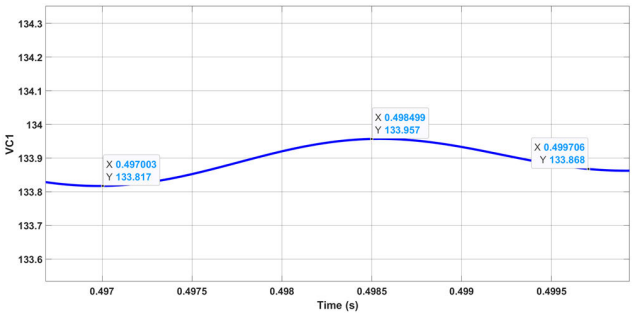

FIGURE 15. Simulation of v_{C1} in MATLAB.

$\Sigma - \Delta$ Illustrating the output voltage considering the following parameters of the QBC:

Being the steady state voltage represented by

$\overline{X_4} = 0, 25\ \overline{v_2} = 48v\ y\overline{X_1} = corrient$

$\overline{i_1} = 3, 7022A$ with $\overline{X_2} = \overline{U_{av}} = \sqrt{48} y \overline{X_3}$ = the voltage $\overline{v_1} = 135.05v$ and $\overline{i_2} = 10, 4167A$

Figures 17 and 18 contain the response to the passivity-based control PBC script and a PI adjustment on its output.

This controller uses a PI (proportional-integral) strategy to adjust the inductor current and keep the voltage across the capacitor close to the reference value.

The yellow line d(t) represents the disturbance function, given by step blocks, one of them from 5 to zero and the other from zero to -5, which is sometimes replaced by a square wave pulse generator, the line blue y(t) contains the controlled variable or output of the System, adjusted to the 48 voltage output, and the signal r(t) in red contains the setpoint or the reference of the desired value, the green line or e(t) contains the error signal, and finally, u(t) with the violet signal, is the input or signal of the controlled pulse to the system

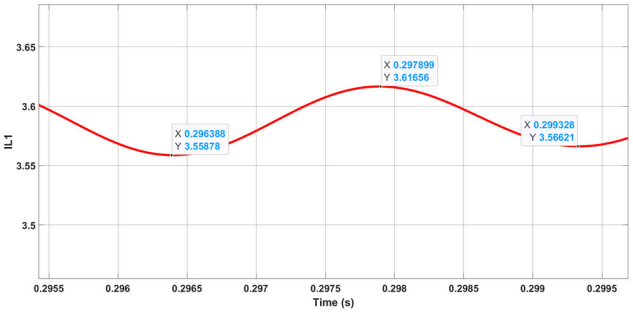

FIGURE 16. Simulation of I_{L1} in Matlab.

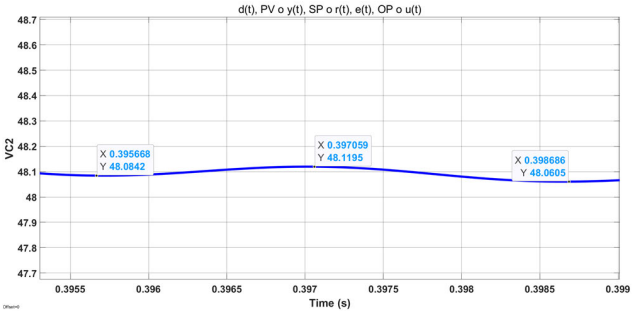

FIGURE 17. Simulation of V_{C2} in Matlab.

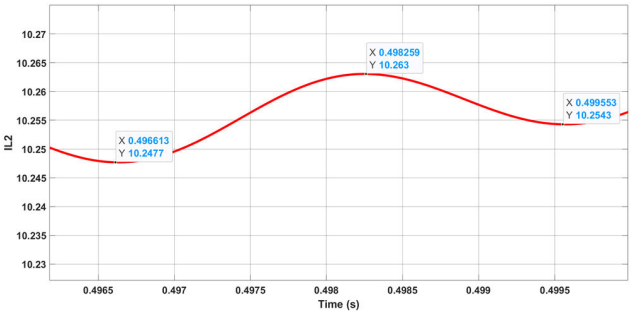

FIGURE 18. Simulation of I_{L2} in MATLAB.

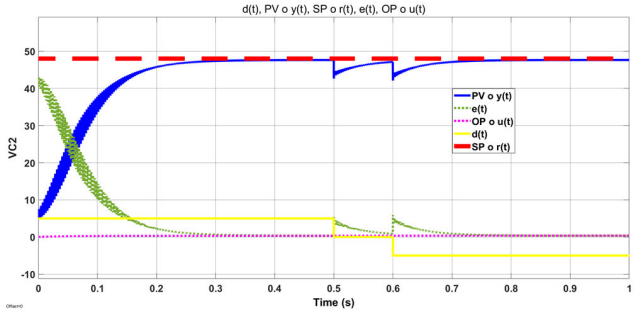

FIGURE 19. Response output V_{C2} and its validation using the pulse generator in the disturbance.

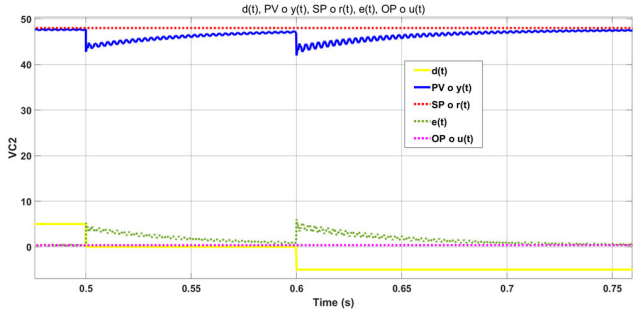

FIGURE 20. Closed loop response with passivity controller.

Considering MCC and the operating points of the response for the stability of the System, the following Figure 15 is considered:

presents the response v_{C1} obtained in Figure 15.

The current I_{L1} can be seen in Figure 16.

In the case of V_{C2}, the response can be seen in Figure 17. It does not reach the expected value, but the response is very close to the expected one, for this case the delta is:

Lastly, the value of Δ_{IL2} can be seen in Figure 17.

The closed-loop passive response obtained by the system simulation can also be observed.

Employing a pulse generator with a constant 5 VDC amplitude in which the disturbances are verified to the same considerations for the validation of the graphs.

Finally, the initial disturbance variation characterized by the two steps blocks, initially described, is presented.

X. EXPERIMENTAL DEVELOPMENT

The experimental development contains two parts, the first is the design of the printed circuit of the QBC, based on the IPC manufacturing standards, to obtain the actual implementation of the System or plant, in which the three control laws are also validated. studied in this present article, this first part will not be given much relevance for the moment, since the intention is the compare the design times and phases for the Development of the System, therefore the main objective of the article is to validate the rapid prototyping design, which is the second part of Experimental Development.

A. DESIGN OF THE PRINTED CIRCUIT

The Printed Design is made by using the IPC (Association Connecting Electronics Industries) standards can be important in most of these phases, especially in the design and manufacture of the electronic card, the IPC standards set standards for the quality and performance of electronic cards, which can help ensure the reliability and safety of the product, within the technological features that it manages, such as the selection of components for IPC standards, define the requirements for electronic components and can help to select the right items. The main active components that were used in the development of the card are the following:

On the other hand, the design of the PCB (printed circuit board) is carried out in the ORCAD program, according to the IPC standards, where the requirements for the design of the PCB are established, including requirements such as pin density, the separation between conductors, the dimensions of the perforations, among others.

Regarding manufacturing, the IPC standards establish the requirements for the manufacture of the PCB, including the requirements for the quality of the materials, the tolerance

TABLE 3. Components used in the design of the QBC.

component	Characteristic	Reference
Diode	high-speed diodes, 600 V, 15 A	MUR1560
Diode	Amp Schottky 20V to 100V	SK310A-LTP
power regulation	integrated circuits of the driver stage 5 V to 3.3 V, 1 A	RFM-0505S
high gain, low drift instrumentation amplifier	programmable gain from 1 to 10,000 and a bandwidth of 200 kHz	AMC1200
high-speed op amp.	3GHz bandwidth and a slew rate of 7000 V/µs.	THS4524_H
voltage converter	9 to 36 VDC at a voltage output of 15 VDC with a maximum current of 1.2 A	VQA-S9-D15-SIP1
switching regulator	voltage in 28V, voltage output, range of 0.8V to 24V, maximum current of 2.5A	TPS54286PWP
precision adjustable voltage reference	Reference 25 V, operation 100 mA.	ATL431LIBQDBZRQ1
Velocity control	2.7V to 5.5V, Current 50 mA	TC654
Hall effect current sensors	5A, 20A or 30A 4,5 V y 5,5 V 10 mA	ACS712
semiconductor power module	600 V, 54 A.	IRGP4660D
MOSFET semiconductor	100 V, 80 A	CSD18535KTT

of the perforations, and the quality of the soldering, among others.

The tests and verification are carried out concerning the IPC standards, and the requirements for the tests and verifications are established, including electrical, mechanical, and operational tests.

Using IPC standards can help ensure that electronic card design and manufacturing meet standards for quality and performance and improve the reliability and safety of the final product.

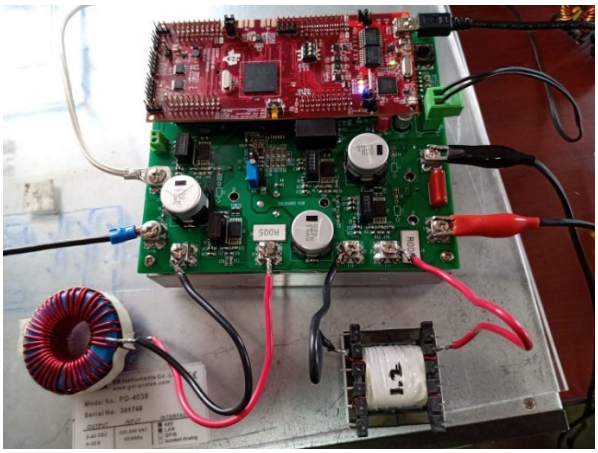

FIGURE 21. Implementation and testing of the QBC.

Finally, and by the conventional validation processes, the testing and verification of the control strategies are programmed in a DSP-Launchxl-f28379d, to illustrate them in a future publication, whose responses are very similar to the simulations, However, not as accurate as those in the rapid prototyping below.

The experiment encompasses dual perspectives. Initially, it aims to scrutinize the timeline involved in the industrial design and implementation of an electronic card meeting all appropriate technical norms and specifications. This involves the entire process from design and simulation to assembly and testing, incorporating proposed controls such as sliding mode and passivity. This approach contrasts with verifying the simulation conducted within the Control Desk of the dSpace CP1103, effectively minimizing expenses on unnecessary material testing, and lengthy selection processes of elements after exhaustive reviews of technical datasheets containing information possibly required for implementation. Additionally, it reduces the need for component wear tests, thermal dissipation trials, assessment of maximum voltage and current, cutoff points, and saturation, among others.

The second perspective focuses on utilizing the implemented card in direct tests with the dSpace CP1103 via rapid prototyping. While the dSpace simulation algorithms yield outputs closely resembling reality, DSpace allows the connection of the card to the DAC and ADC ports, acting as an interface between the control signal input by the PWM signal and the system's feedback. This facilitates real-time measurement of output signals using an oscilloscope, despite the algorithms' high fidelity to real responses.

B. RAPID PROTOTYPING DESIGN

To carry out the experimental development, the dSPACE CP1103 tool was considered, due to the benefits and characteristics it offers in rapid prototyping, in RT in the face of system disturbances.

dSPACE is a company that offers a variety of tools and solutions tales for system development. Its products include simulation and test systems (such as MIL, HIL, and SIL), automotive control systems, and process control systems, among others.

DSPACE offers a platform for the integration of the different elements in a single platform, which facilitates the task of using MIL, HIL, and SIL through rapid prototyping, since it is possible to simulate a complete system with different levels of abstraction, from mathematical modeling to actual hardware. It also allows a direct connection between the mathematical model and the hardware, allowing design validation in RT.

In addition, dSPACE offers many libraries, tools, and functions to facilitate the simulation and testing process, which allows for reduced development time and increased system reliability.

The various results are illustrated below, through the validation of rapid prototyping in RT, in which each of the controls is implemented, such as sliding mode control SMC and passivity-based control PBC, then the output variations concerning disturbances of 100 Hz and 500 Hz are shown.

The rapid control prototyping experiment consists of two parts. The first part involves the execution of simulations performed on the Control Desk interface, which constitutes the software in the loop of the dSpace. This desktop environment contains all the necessary configurations to conduct simulation schemes, like Simulink in MATLAB. It enables observing the behavior of the simulated signal, verified through the output connected to an oscilloscope via the DAC ports.

The initial segment entails the construction of each control simulation. The first control, sliding mode, constitutes the simulation and the embedded system in graphs E1 and E2, utilizing double-loop feedback and digital output. Subsequently, two types of disturbances are introduced, one at 500Hz, as depicted in Figure 31. The aim is to measure how power supply noise, caused by voltage fluctuations or noise in the power source, might affect circuit performance, potentially stemming from the electrical grid or other devices connected to the same power source.

Electromagnetic Interference (EMI), like wiring from the power source, can capture electromagnetic interference, particularly in industrial settings or with nearby high-power equipment. The second disturbance, at 100Hz, focuses on output load, influenced by potential environments:

Load Noise: The circuit's connected load can cause output fluctuations or interferences, especially in critical applications such as audio electronics or communication systems.

Output Impedance: The circuit's output impedance can impact energy transfer to the load. Ensuring appropriate impedance for the load can be crucial.

Filter and Regulator Verification: Some input/output filters can assist in reducing input/output circuit noise.

This control, regarding current control, utilizes voltage regulation as a reference to maintaining stable output, even with input variations. The simulation may address cable types and their quality to ensure solid connections that minimize input and output circuit-related issues. Shielding is highlighted as crucial in environments susceptible to electromagnetic interference, as shielding in certain circuit parts can be beneficial.

These considerations are critical elements for potential excellent switch construction by the manufacturer. The simulated tests for the subsequent passivity-based control were conducted based on graph G1, aligning the MATLAB Simulink simulation graph to the Control Desk graph, and adjusting the required algorithm to obtain system-specific outputs, as seen in figure 34.

The disturbances of the system are determined from Figure 35, one in the system's input environment with 500Hz signals (figure G5) that measure the control's robustness against voltage fluctuations or power supply noise. The other, at 100Hz (figure G4), deals with intermediate and output interferences such as load noise, output impedance, filter verification, regulators, cables, and shielding, previously explained to simulate real environment conditions.

The second part employs the implemented card directly with the dSpace CP1103, connecting the control simulator output to the IRGP4660D-EPBF input signal and directly connecting the output to the oscilloscope. Testing disturbances are notable, as 500Hz input perturbations are taken, commonly found in audio, communication, and interference source scenarios. Similar conditions apply to output effects, where real effects determine 100Hz perturbations.

Following these, two controls are measured. The first, in sliding mode control, depicted in Figure 22, demonstrates a gradual change in the duty cycle automatically with resistance variation of 3.3, 4.7, and 5.1 ohms. This is validated through the SIL present in the algorithm that manages the simulation effect in the Control Desk, resulting in an output of 47.97 VDC, closely matching the suggested value in the simulation.

Finally, the output is measured concerning passivity-based control using the designed card or square buck for two signals that similarly power the IRGP4660D-EPBF input switch. The first applies a maximum load value of 5.1 ohms, and the second, a minimum load of 3.3 ohms. It illustrates how, thanks to the SIL program algorithm present in the Control Desk simulation, an automatic adjustment in the duty cycle percentage demonstrates a real output signal on the oscilloscope of 48.11 VDC.

This work has benefited from significant contributions from related works, including [45], which proposes a fractional control scheme with a self-generating recurrent fuzzy neural network to mitigate harmonic distortions. Their fractional approach reduces 'chattering', and the SCRFNN enhances adaptability to uncertainties, standing out for its effectiveness in harmonic suppression and robustness.

Likewise, in [46], an adaptive super-twisting controller with a nonlinear state observer is presented to enhance the performance of the active power filter. This approach achieves high precision in current compensation and significantly reduces 'chattering'.

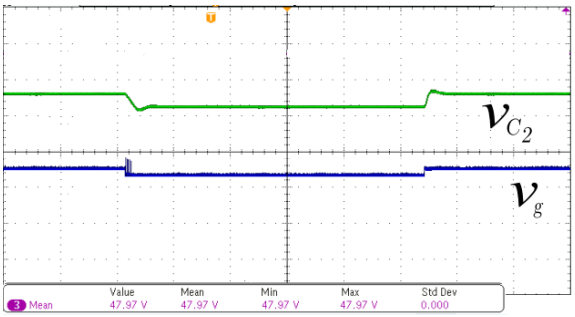

FIGURE 22. SMC oscilloscope output with 380 VDC input power supply.

In [47], a controller is developed with fuzzy neural networks, wavelets, and super-twisting sliding modes to improve power quality in an active power filter. The combination of these techniques allows precise control of currents and harmonics, validated through hardware experiments under nonlinear conditions and uncertainties. This research offers valuable insights for various applications.

C. QBC UNDER DIFERENT LOADS

Since the real results are very similar to the experimental ones in the rapid prototyping responses testing the three controls in dSPACE 1103, the validation of the load change is carried out with the SMC, to avoid biases due to any of the robust controls, with a power of 500 W, a circuit or a low-pass filter with a frequency of 10 KHZ was incorporated into the card or plant to attenuate the noise in the output voltage, in the test of the type II PI controller, for load change, a ISO5452-Q1 A driver configured with a time of 100 ms, with a 15 VDC floating supply, is used to power the integrated circuit. In Figure 22 you can see the variation of the real load of 4.98 A when using the Slider control with resistors of 3.3 ohms, 4.7 ohms, and 5.1 ohms to ensure a response in the output voltage of 47.97 VDC.

To determine the voltage spike during the load change transition, the oscilloscope setup is set to attenuate the direct current (DC) component of the signal and measure the maximum and minimum values of the voltage. In the face of load change in RT, the inverter maintains its permanent voltage state of 48.11 VDC.

Figure 23 shows a regulated electrical output of 48.11 VDC, with a recovery of 100 ms. You can also see in Figure 37, (a) a maximum peak of 2.96 VDC, and a minimal peak of −2.96 Figure 23, (b) along with a converter recovery time of approximately 100 ms in voltage variation. load, and like the SMC experiment, the variation was carried out with resistances of 3.3, 4.7, and 5.1 ohms, and with a load of 4.98A. These results support the correct implementation of the controller and validate the solution presented in the project.

XI. ANALYSIS OF RESULTS

Below is a table with information on the results regarding the parameters for each of the controls.

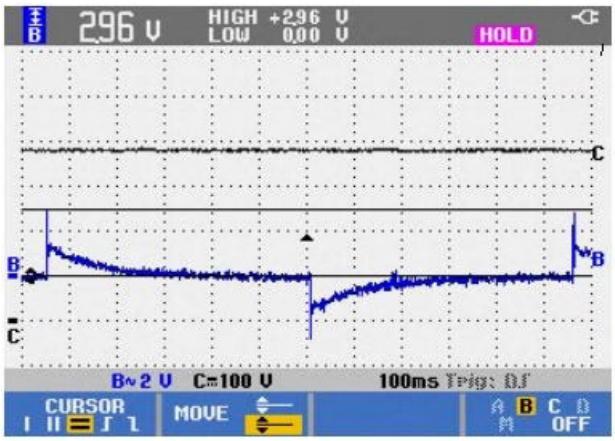

(a) Closed-loop oscilloscope output PCB with maximum value on load change.

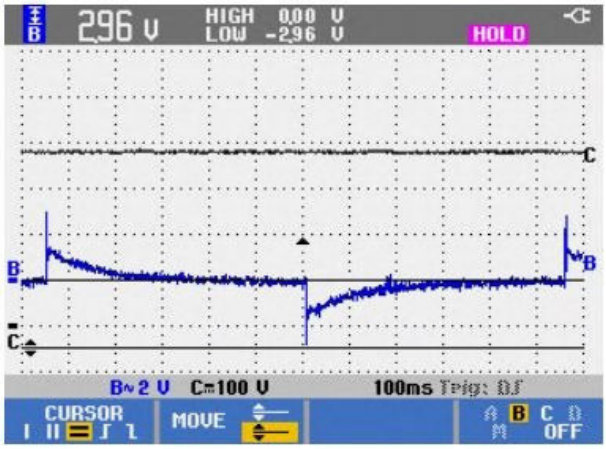

(b) Closed-loop oscilloscope output PCB with the minimum value on load change.

FIGURE 23. PCB oscilloscope output with the maximum and minimum value on load change.

According to the previous table 4, the values of the controls that are most like the references obtained theoretically are varied. In the case of $\boldsymbol{vc_1}$ with a reference of '135.0555', in the case of $\boldsymbol{iL_1}$ reference '3.7022', the closest is the sliding mode control SMC that reaches '3.41169', in a time of '0.0360023', with an overshoot of up to '4.40851' whose oscillation.

it is compensated with a duration of '0.0360165', which is a very small variation concerning the ripple, the behavior of $\boldsymbol{iL_1}$ is also favored in the passivity-based control PBC, however, it starts a little earlier at '3.55878' for '0.296368' and in short times estimated by the two controls, the approximation is minimal and only reaches '3.61656' in a time of '0.299328' s.

In the case of $\boldsymbol{iL_2}$ with a reference of '10.4167', the one who reaches a close value faster is the passivity-based control PBC with '10.2477', in only '0.496613' s, however, it reaches '10.263' in '0.499553', the response is a little less fast compared to the slider, which starts earlier, with '10.8234' in '0.0349129' s, but reaches values a bit higher than '12.4289', in only '0.0349272' s.

TABLE 4. Values for the parameters in each controller.

Controller measurement						
Slider Mode						
	min	max	dif	t min	t max	dif
vc1	127,733	127,915	1,82E-01	0,0360637	0,0360778	1,41E-05
il1	3,41169	4,40851	9,97E-01	0,0360023	0,0360165	1,42E-05
il2	10,8234	12,4289	1,61E+00	0,0349129	0,0349272	1,43E-05
vc2	47,9835	48,0127	2,92E-02	0,0344483	0,0344626	1,43E-05
Passivity						
	min	max	dif	t min	t max	dif
vc1	133,817	133,957	1,40E-01	0,497003	0,499706	2,70E-03
il1	3,55878	3,61656	5,78E-02	0,296368	0,299328	2,96E-03
il2	10,2477	10,263	1,53E-02	0,496613	0,499553	2,94E-03
vc2	48,0842	48,1195	3,53E-02	0,395668	0,398686	3,02E-03

Finally, for the output Vc2 of reference '48', which manages to arrive more precisely is the control by sliding mode control SMC, starting at '47.9835' with only '0.0344483' s, adjusting to the value of '48.0127' at '0.0344626' s. Next to this would be the passivity-based control PBC which starts with a very close value of '48.0842 in '0.395668' s, and only reaches '48.1195' in '0.398686' s.

A. PERFORMANCE INDEX

Control performance indices are measures used to assess the performance of a control system in each process. These indices can be used to compare different control systems and to determine the success of a control system in meeting established objectives. Some include response time, accuracy, stability, and robustness [40], [41].

B. PERFORMANCE INDICES

Several performance indices can be used to measure the performance of a control process. Some common examples include Performance Index (PI), Capability Index (Cp), Enhanced Capability Index (Cpk), and Z-Performance Index (Z-score). The Performance Index (PI) is a measure of the quality of the process and is calculated as the difference between the desired value and the current value, divided by the desired value [42]. The Capability Index (Cp) is a measure of the ability of the process to meet tolerance requirements and is calculated as the difference between the upper limit and the lower limit of tolerance, divided by twice the process standard deviation.

Enhanced Capability Index (Cpk) is a measure of the ability of the process to always meet tolerance requirements and is calculated as the minimum value of Cp and the quality capability index (Cpk = min (Cp, CPU)).

The Z performance index (Z-score) is a measure of how far a specific value moves from the expected value and is calculated as the difference between the expected value and the current value, divided by the standard deviation of the process [43]. The basic indices, PI, Cp, CpK, and Z-score, are represented in Table 5.

A PI greater than 1 indicates that the process is operating above the desired value, while a PI less than 1 indicates that the process is operating below the desired value. A PI close to 0 indicates that the process is operating close to the desired value, taking this principle into account, there are various values very close to zero, for the three controls, in the

TABLE 5. Performance indices, PI, Cp, CpK, and Z-score.

Experimental performance index				
Slider Mode				
	PI	Cp	Cpu	Z score
vc1	1,35E-03	-0,001981786	0,001763646	117,921476
il1	2,69E-01	-0,074280711	0,056753177	-1,79104797
il2	0,154127507	-0,129794539	0,122903768	-4,26145462
vc2	6,08E-04	-1,76757E-05	5,45104E-05	-1,71242441
Passivity				
	PI	Cp	Cpu	Z score
vc1	1,04E-03	4,091489918	4,188411845	0,52891368
il1	1,56E-02	0,020492319	0,023344054	0,04123456
il2	0,001468795	0,095134876	0,096749962	0,00120805
vc2	7,35E-04	0,021837896	0,023628221	-0,78539784

case of v_{C1}, it can be affirmed that it is very close to zero. in the three controls, however, it is closer to the case of the passivity-based control PBC, with '1.04e-03' followed by the sliding mode control SMC fix with '1.35e-03', for iL_1 is smallest in passive with '1.56e-02', followed by sliding mode control SMC with '2.69e-01'.

For iL_2, the closest value to zero is the passivity-based control PBC with '0.001468795', followed by the slider with '0.154127507'.

Finally, for Vc2, the smallest value is that of the sliding mode control SMC with '6.08e-04', followed by passivity-based control PBC with '7.35e-04'.

A Cpu value greater than 1 indicates that the process has enough capacity to meet the tolerance requirements. A value less than 1 indicates that the process does not have enough capacity to meet the tolerance requirements. According to the values in Table 5, it can be said that they are very close to 1, however, the most relevant ones are worth the Worth noting.

A high Z-score indicates that the value is significantly higher than the expected value. A low Z-score indicates that the value is significantly lower than the expected value, the typical case that covers all cases is control for passivity-based control PBC, since for v_{C1} it registers '0.52891368', for iL_1 it has '0.04123456', being the lowest of iL_2 with just '0.00120805', which is not a very relevant value, followed by this control we find the slider modes that in v_{C1}, has a Z-score value of '117.921476'.

Performance Indices (ISE, ITSE, IAE, ITAE):

Below are the most important results regarding the analysis of the behavior of performance indices, according to the most used at the industrial level.

From the previous indices, the ITAE is chosen, since it is a performance measure that is used to evaluate the control of process control systems. It is a measure of the time absolute error integral and is used to assess the effectiveness of a controller in terms of how quickly error is corrected and the stability of the system. In switching converters, the ITAE is especially important as it is used to assess controller performance in terms of how quickly system stability is reached and the level of distortion in the system. Using ITAE allows controller designers to optimize system performance in terms

TABLE 6. ITAE performance indexes.

ITAE INDEX	
Slider Mode	
ITAE	
vc1	1,02E-03
il1	3,90E-05
il2	1,76E-04
vc2	1,34E-06
Passivity	
ITAE	
vc1	1,93E-01
il1	1,65E-02
il2	3,15E-02
vc2	1,05E-02

of stability and distortion, resulting in a higher quality and more reliable system.

C. INTEGRAL OF TIME MULTIPLIED BY ABSOLUTE ERROR CRITERION (ITAE)

The Multiplied Time Integral Absolute Error (ITAE) criterion is a measure used in process control to assess the variability of a process over time. It is calculated as the time integral multiplied by the absolute difference between the desired process value and the measured process value.

The multiplied time integral absolute error criterion is often used in control by attribute (CA) analysis to evaluate the performance of a process. By including time in the calculation, the ITAE reflects not only the variability of the process but also the time elapsed from when a change is made to the process until an acceptable level of stability is reached.

To calculate the ITAE for this process, we can use the following formula: ITAE $= \int$ t |xi – x_wanted| dt [44].

Where: t is the time elapsed since a process change is made, xi is each of the process measurements, and ''x_wanted'' is the desired value of the process.

A small value of the Multiplied Time Integral Absolute Error (ITAE) criterion. The ITAE is used to assess the variability of a process over time, and a low value indicates that the process is stable and has little variability. In general, the lower the ITAE value, the better the performance of the process. However, it is important to note that the ITAE is not the only measure that can be used to assess the performance of a process and that it may be necessary to use several different criteria to obtain a complete picture of the performance of the process, accordingly., it can be seen in Table 6, that almost all the variables of all the controls have stable behavior, however, it is worth noting that for $\boldsymbol{v_{C1}}$, the sliding mode control with '1.02e-03', continuing passivity with '1.93e-01', for $\boldsymbol{iL_1}$ again sliding mode control SMC with '3.90e-05', and finally passivity with 1.65e-02', for $\boldsymbol{iL_2}$ there is again a sliding mode control SMC with ''1.76e-04', to end passively with '3.15e-02', and finally for the Vc2 output there is a sliding mode control SMC again with '1.34e-06', and finally the passivity of '1.05e-02'.

D. GENERAL CONSIDERATIONS

The response time it takes for the Slider Mode Control System to respond to the input signal to reach the desired 48 VDC value is approximately 0.046 s in steady mode, with a Type II PI operating in a dual loop, rated tracking that responds to a speed of fewer than 0.01 s, however, the overshoot decreases at a considerable speed, after a disturbance of 5 VDC that generates a small very fast overdamped oscillation, managing to stabilize in permanent mode after 0.0465 s, showing a behavior sensitive to change as can be seen in figure 10 and following, where the design model is tested by driving a controller, which in turn is reflected in the experimental response through the use of the dSPACE CP1103, as can be seen in the electrical response of figure 31, 32, and its HIL and SIL simulation in figure 30.

The precision in the output of the desired value for the control implemented in sliding mode control SMC, there is a ripple with values between 47.9835 and 48.0127 VDC in times of 14.30 μs, as can be seen in Figure 16, finding in these results very close values. desired in short response times. The efficiency of the System in terms is equivalent to the input power of 500.002472 and the output power of 500.0016, having a relationship of 99.999826%.

At the experimental level, two tests were carried out, with disturbances of 100Hz and 500Hz, by using the simulation with the Control Desk tool of the dSPACE CP1103, as illustrated in figures 28 and 29,30 in its rapid response in RT, where the robustness of the control in sliding mode control SMC can be evidenced, due to the observed sensitivity to disturbances.

The passivity model contains a dynamic in which the response time is obtained by seeking immediate stability from approximately 0.3 s, for the tests carried out with disturbances between -5 VDC and 5VDC during periods of 0.5 and 0.6, during which its rapid recovery of almost 0.1 s for each disturbance can be observed, as shown in figure 27, which, similar to the control in sliding mode control SMC, presents robustness against any disturbance, as evidenced in figure 23, compared to a sequence of 5 VDC pulses, where the sensitivity to disturbance is sensitive since it stabilizes the signal quickly in times of approximately 0.1 s.

The signal pressure is evidenced in the ripple, which has a range between 48.0842 and 48.1195, reaching values very close to the reference in times of 3,018 ms.

At the experimental level, two perturbations are also carried out with dp1103, one with 100Hz, which is observed in Figure 36, made using the control desk tool, and with an electrical behavior.

hand with the disturbance of 500Hz, whose simulation in the control desk is observed in Figure 37, with electrical output, it can be said regarding the above, that the control

by passivity is also robust mainly due to its sensitivity to high frequencies.

SMC is well-known for its ability to achieve accurate reference tracking and rapid response to disturbances. However, it may be more susceptible to vibration issues, characterized by rapid oscillations in the control signal, and may require fine-tuning of controller parameters for optimal performance, see Figure 36.

On the other hand, PBC can be highly effective in terms of stability and robustness, particularly in certain cases. Nevertheless, its performance can be influenced by the choice of controller parameters and the precision of system modeling. In our developed model, it exhibited favorable behavior, as shown in Figure 37.

There are several reasons why it is important to do multiple control performance indices, such as the PI index, CP index, CPK index, and Z-score: They provide a more comprehensive view of control system performance. By using multiple performance indices, you can get a more complete picture of control system performance and detect problems that might not be apparent using a single index. Help identify specific problems. By using various performance indices, you can more accurately determine which issues are affecting control system performance and take corrective action. They allow the performance of different control systems to be compared. By using various performance indices, you can compare the performance of different control systems and determine which is best suited for a given application. They help improve efficiency and productivity. By using various performance indices, problems can be identified and fixed to improve control system efficiency and productivity.

XII. CONCLUSION

The benefits of rapid prototyping that can be highlighted in this document are:

Allows for early testing of the design: Rapid prototyping allows a physical version of the design to be built as soon as possible, allowing problems to be detected and corrected early in the development process.

Facilitates communication: The physical prototype allows for better communication between the development team and customers or end users, as it is easier for them to understand and provide feedback on a tangible design.

Reduce Costs: Building a prototype early helps catch problems before the design is finalized and expensive components are incorporated, which can help reduce costs in the development process.

Improves efficiency: Rapid prototyping allows for continuous iteration and continuous improvement of the design, which increases efficiency in the development process and improves the quality of the final product.

Facilitates decision-making: The physical prototype allows the development team and customers or end users to evaluate the design and make informed decisions about necessary changes or improvements.

dSPACE offers a comprehensive, integrated platform for system development that facilitates the use of MIL, HIL, and SIL through rapid prototyping. This allows engineers to perform testing and validation at different levels of abstraction, helping to reduce development time and increase system reliability.

In performance indices Passivity-based control PBC generally outperforms sliding mode control SMC in maintaining desired values for the controlled parameters, with significantly lower PI values across multiple parameters (e.g., Vc1: PBC PI = 1.04e-03, SMC PI = 1.35e-03).

Notably, there is a substantial deviation from the expected value for Vc1 under sliding mode control SMC, as indicated by a high Z-score (Vc1 SMC Z-score = 117.921476).

Further investigation is required to assess the practical significance of these deviations, particularly in the case of Vc1 under sliding mode control SMC, to understand their potential implications and the need for adjustments.

A low Multiplied Time Integral Absolute Error (ITAE) criterion indicates process stability and minimal variability over time. The values in Table 6 demonstrate stable behavior for most variables in all controls. Notably, for Vc1, sliding mode control records '1.02e-03' while passivity-based control shows '1.93e-01'. In the case of iL1, sliding mode control SMC achieves '3.90e-05', and passivity-based control reaches '1.65e-02'. for iL2, sliding mode control SMC registers '1.76e-04', while passivity-based control exhibits '3.15e-02'. Finally, for the Vc2 output, sliding mode control SMC records '1.34e-06', and passivity-based control reaches '1.05e-02'. These values collectively indicate the stability and performance of the controls for their respective variables.

In general form, the Slider Mode Control System's response time reaches 48 VDC: Approximately 0.046 s in steady mode with a Type II PI operating in a dual loop.

Overshoot after a 5 VDC disturbance: A small, very fast overdamped oscillation stabilizes in approximately 0.0465 Precision in output for sliding mode control SMC: Ripple between 47.9835 and 48.0127 VDC with 14.30 μs intervals, achieving values very close to the desired response.

System efficiency: Input power of 500.002472 and output power of 500.0016, with an efficiency rate of 99.999826%.

Passivity model's response time to disturbances: Immediate stability was achieved in approximately 0.3 s, with rapid recovery of almost 0.1 s for each disturbance.

Passivity model's sensitivity to disturbances: Stable signal in approximately 0.1 s in response to 5 VDC pulses.

The exploration undertaken through the design, assembly, and validation of the QBC underscores the pivotal role of rapid prototyping in modern control systems development. By juxtaposing the traditional methods against the accelerated, iterative approach facilitated by dSPACE, our study delineates a tangible roadmap towards cost-efficiency, enhanced communication, and robust design validation. The comparative analysis accentuates the reduction in development time from six months to approximately one week during the MIL, HIL, and SIL validation stages, elucidating

a significant stride towards agile development practices in control engineering. Furthermore, the insights garnered from the performance indices in the analysis section elucidate the potential for optimizing control parameters to achieve superior system reliability and responsiveness. While the results are promising, a deeper exploration into the scalability of the rapid prototyping approach, and its applicability across diverse control systems, is warranted for a more comprehensive understanding. The potential limitations and the scope for future investigations to further refine the control laws and evaluate alternative rapid prototyping platforms also merit discussion, paving the way for advancing the state-of-the-art in control systems engineering.

Future Works: This methodology could also be assessed with other types of control laws, either using robust controls or classical control. Likewise, validation could be performed using various industrial plants, testing high-performance values in conditions that cover different voltage ranges.

The real-time experiment alternately consolidates the initial simulation given in the Control Desk, starting from its output delivered to the oscilloscope, which should closely resemble using a physical plant in the form of an interface connected to the dSpace, transferring its output to the software's feedback, and again, its actual output delivered to the oscilloscope. Verification of current and voltage must be very close, as well as response times in the system. This validation can be deeply explored in the results analysis section.

To determine the parameters of the controller in sliding mode, the parameters were adjusted near a specific point, validating the robustness of the controller with different loads. The system has an inner loop with a sliding mode switching surface and an outer loop with a proportional-integral (PI) controller. External control is designed using the transfer function equation (97) and a PI compensator. The system loop gain is expressed through the classical pole assignment technique, as illustrated in Section VII, Section D.

The transfer function of a combined proportional-integral controller in the Laplace domain mainly aims to select kp, ki to achieve optimal performance of the control system. These parameters are typically adjusted using tuning methods to meet specific system requirements in terms of stability, response time, and disturbance attenuation.

$$T(s) = G_{v2i_{ref}}(s)\left(k_p + \frac{k_i}{s}\right) = \frac{v_2(s)}{i_{ref}(s)}\left(k_p + \frac{k_i}{s}\right) \quad (183)$$

$$1 + T(s) = s^4 + (\alpha_2 + \beta_2 k_p)s^3 + \left(\alpha_1 + \beta_1 k_p + \beta_2 k_i\right)s^2 + \left(\alpha_0 + \beta_0 k_p + \beta_1 k_i\right)s + \beta_0 k_i \quad (184)$$

Therefore: $\left(\alpha_2 + \beta_2 k_p\right) = \gamma_3$ $\left(\alpha_1 + \beta_1 k_p + \beta_2 k_i\right) = \gamma_2$ $\left(\alpha_0 + \beta_0 k_p + \beta_1 k_i\right) = \gamma_1$ $\left(\beta_0 k_i\right) = \gamma_0$

The variables are then substituted into the equation.

$$1 + T(s) = s^4 + \gamma_3 s^3 + \gamma_2 s^2 + \gamma_1 s + \gamma_0 \quad (185)$$

According to the Routh-Hurwitz criterion, we have (186), as shown at the bottom of the page.

To determine stability, it can be affirmed that almost all elements in the first column have the same sign. According to the Routh-Hurwitz criterion, the system could be considered stable. This is further confirmed through pole assignment, deducing from the roots of the characteristic polynomial that their real parts are −9.9946, −0.2127, and −0.2127. All real parts are negative, indicating that all roots have a real part less than zero.

Therefore, according to the pole placement criterion, the system is stable, consistent with the Routh-Hurwitz criterion that provided an ambiguous signal. Locating the poles in the complex plane is a more precise method of evaluating system stability.

Overall, according to Figure 6, the Bode plot description indicates that the system, with the incorporated PI controller, exhibits a rapid response to frequency changes, high gain within a significant frequency range, and a negative phase suggesting a slight delay.

Thus, upon computing values for this internal PI, they are tuned to Kp=0.952510 and Ki=952.51000.

Finally, aiming for coherence, the controller's robustness is evaluated across a power range from approximately 100W to just over 1100W. The results are depicted in Figure 10, showing that despite equilibrium variations, performance remains consistent, ensuring stabilization time throughout the power range.

$$\begin{vmatrix} 3554 & 19740000000 & 1042 & 701800000 \\ -149600 & 1 & 744700 & 0 \\ \frac{1476552000001777}{74800} & \frac{1273885}{68} & 701800000 & 0 \\ \frac{1686182515601777}{1476552000001777} & \frac{1107441472545323331900}{1476552000001777} & 701800000 & 0 \\ -\frac{2186089466803940343562895364 8366}{1686182515601777} & 701800000 & 0 & 0 \\ \frac{8198038871067400182692856570518380100}{109304473340197017178144768241 83} & 0 & 0 & 0 \\ 701800000 & 0 & 0 & 0 \end{vmatrix} \quad (186)$$

To determine parameters for the passivity-based controller, stability is determined using Lasalle's asymmetric stability theorem. This theorem outlines conditions under which the system evolves toward an invariant set, regardless of initial conditions, and this set attracts all system trajectories. As explained in Section XIII D, passivity control is a technique using the idea of passivity rather than state feedback. Passivity implies the system won't draw more energy than supplied, beneficial for stability and system performance. Using canonical forms in combination with passivity control relates to representing the system in a specific form facilitating controller analysis and design. Canonical forms like controllable canonical form and observer canonical form offer standard system representations aiding in understanding properties and controller design, described in Sections IX-A and IX-B.

Finally, akin to sliding mode control, the system incorporates an internal loop operating through passivity-based control and an external loop with a proportional-integral (PI) controller, as illustrated in Figure 27. It's configured by tuning for a stable system with Kp= 0.001256 and Ki= 0.100933, respectively

In the experiment and simulation, the comparative study between the proposed method and other methods is expected to demonstrate the effectiveness of the proposed method.

During the experiment and simulations, it is anticipated that the comparative analysis between the proposed method and other methodologies will evidence the effectiveness of the proposed approach. The results are expected to conclusively reflect improvements in terms of efficiency, system stability, and ability to withstand disturbances, thus reinforcing the suitability and advantages of the proposed method compared to the evaluated alternatives.

During the research, extensive performance analysis techniques were applied, including metrics such as PI, Cp, CpK, Z-score, and ITAE. These metrics were selected to evaluate various key aspects of the system, such as response time, signal accuracy, system stability, and resource utilization efficiency. The inclusion of these metrics strengthens the comprehensive evaluation of the proposed method, allowing a detailed comparison with other approaches and robustly demonstrating the effectiveness and improvements offered by our proposal.

APPENDIX A
APPLICATION OF CALCULATIONS

The purpose of this exercise is to corroborate the calculations made in the previous section. To observe through simulations the effectiveness of the calculations.

It is important to determine the capacitances and inductances, as well as the voltage and current values in a steady state, using the following data:

In principle, the output resistance is calculated:

$$R = \frac{V_{c2}^2}{P_0} = 4.6080\ \Omega \tag{A1}$$

TABLE 7. QBC parameter values.

V_g	V_0	P_0	F_S	$\frac{\Delta I_{L1}}{I_{L1}}$	$\frac{\Delta I_{L2}}{I_{L2}}$	$\frac{\Delta V_{C1}}{V_{C1}}$
$380V$	$48V$	$500W$	$100KHz$	15%	10%	0,5%

TABLE 8. Calculation of parameters quadratic Buck.

$\frac{\Delta V_{C1}}{V_{C1}}$	D	Dp	R
$\frac{\Delta V_{C2}}{V_{C2}}$	sqrt (Vc2/Vg)	1-D	Vc2^2/Po
0,5%	0.3554	0.6446	4.608

Second, steady-state values are calculated according to equation (39), which is calculated $\boldsymbol{I_{L2}}$

$$I_{L2} = \frac{V_{c2}}{R} = 10.4167\ \text{A} \tag{A2}$$

Using equation (34) find the value I_{L1}, calculating before the value D through the equation (49).

$$D = \sqrt{\frac{48}{380}} = 0.3554 \tag{A3}$$

Then

$$I_{L1} = 10.4167 * 0.3554 = 3.7022\ A \tag{A4}$$

Then we proceed to find the values for V_{C1} y V_{C2}, using the equations (30) y (32), knowing that:

$$V_{C2} = V_0 \tag{A5}$$

Therefore:

$$V_{C1} = \frac{48V}{0.3554} = 135.0555V$$

Once the steady-state values have been obtained, the inductance and capacitance values are found.

Starting from the inductance L_2 using equation (43) is equal to:

$$L_2 = \frac{0.3554 * 135.0555V * (1 - 0.3554)}{2 * 100KHZ * 3.7022 * 0.10} = 4.1787e - 04H \simeq 0.4mH$$

for L_1 using equation (41) its value is:

$$L_1 = \frac{0.3554 * 380V * (1 - 0.3554)}{2 * 100KHZ * 10.4167 * 0.15} = 0.2786\ H \simeq 278.6mH$$

Finally, the values of the capacitances are found to find C_1 since by equation (45), it is found that $C_1 = C_2$

$$C_1 = \frac{-0.3554 * 10.4167 * (0.3554 - 1)}{2 * 100KHZ * 135.0555 * 0.005} = -1.7670e - 05F \simeq 177\mu F$$

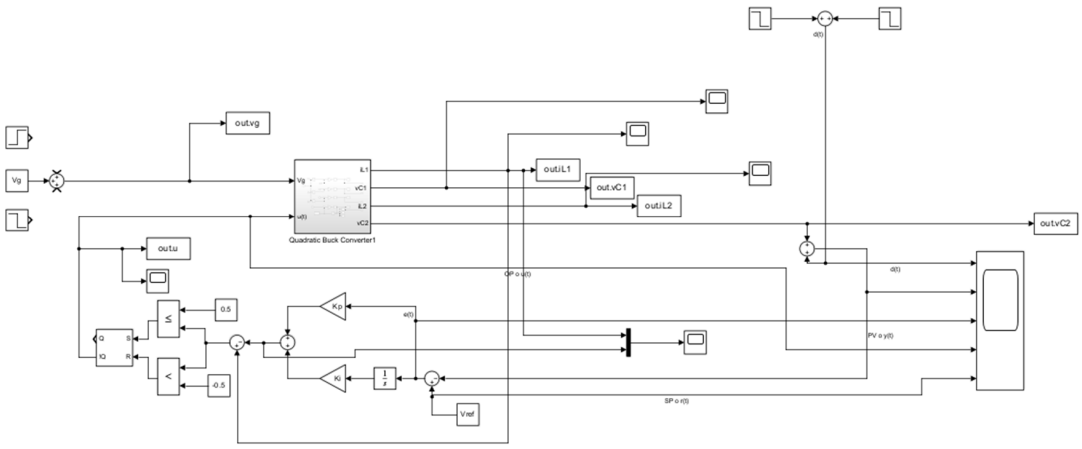

FIGURE 24. Block diagram of the QBC with double slider loop.

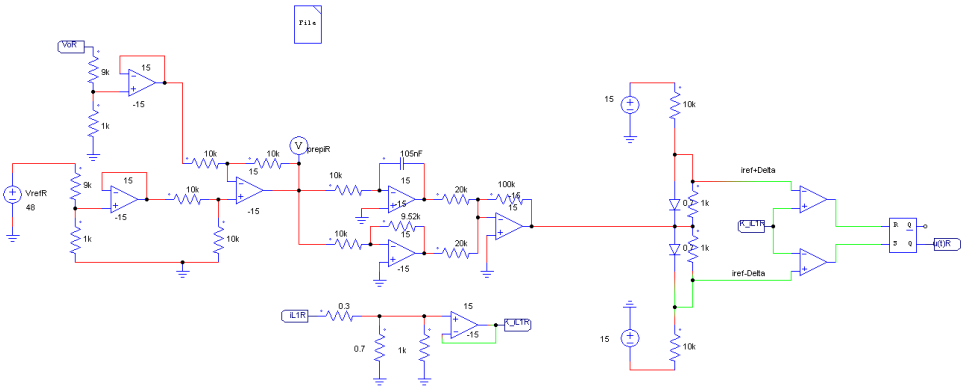

FIGURE 25. Schematic diagram in PSIM of the Type II controller slider mode control.

When selecting the calculated variables, a simulation is carried out in MATLAB, or the block of the quadratic Buck converter that contains the transfer function of the systems, given by the main parameters listed in Table 7 and Table 8.

The voltage output ranges between 135,695 and 134,342; and when calculating the value of the delta, we get:

$$\Delta_{VC1} = \frac{135.695\text{V} - 134.342\text{V}}{2 * 135.0555V} * 100 = 0.5009\%$$

For this case, the delta found is:

$$\Delta_{IL1} = \frac{4.729\text{A} - 2.668\text{A}}{2 * 3.7022\ A} * 100 = 27.8348\%$$

$$\Delta_{VC2} = \frac{48.017\text{V} - 47.937\text{V}}{2 * 48V} * 100 = 0.0833\%$$

$$\Delta_{IL2} = \frac{10.957\text{A} - 9.882\text{A}}{2 * 10.4167\ \text{A}} * 100 = 0.0521\%$$

In the case of the coils, the error is small, which does not bring problems to the construction, on the contrary, we will obtain a better response.

APPENDIX B
ADDITIONAL QBC SMC SLIDING MODE CONTROL DESIGN DETAILS

The behavior simulation program for the QBC is elaborated, in the results are presented in Figure 24.

APPENDIX C
ADDITIONAL QBC SMC SLIDING MODE TYPE II COMPENSATOR CONTROL DESIGN DETAILS

The design of the compensator based on the main circuit for the OP-AM conditioning, the PI, and its feedback circuit is expressed using the Power Simulation PSIM simulation of Figure 25 which feeds the QBC circuit, through the PI control strategy, as shown in Figure 26.

APPENDIX D
ADDITIONAL QBC PCB PASSIVITY-BASED CONTROL CLOSED-LOOP CONTROLLER DESIGN DETAILS

See FIGURE 27.

APPENDIX E
EXPERIMENTAL CONTROL IN SLIDING MODE CONTROL SMC

According to the controller designs, the construction and schematic are modeled in the converter diagrams shown in Figures 7 and 13. Then, based on the experimental design, the plant with which the dSPACE CP1103 tests are validated is started up.

From the MATLAB simulator incorporated in the simulation software incorporated in the dSPACE CP1103 model, the double feedback loop is obtained for the validation of

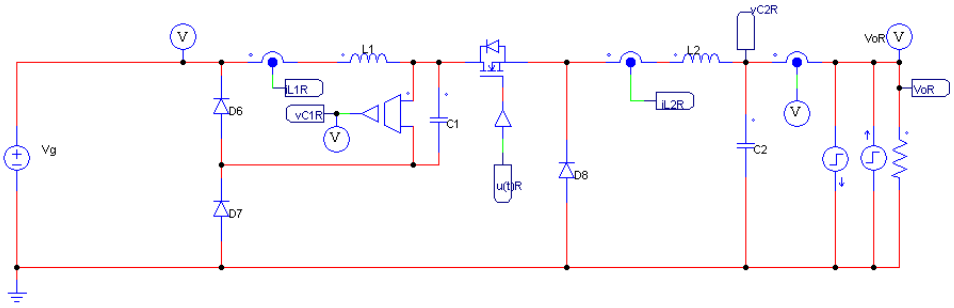

FIGURE 26. QBC configuration diagram in PSIM.

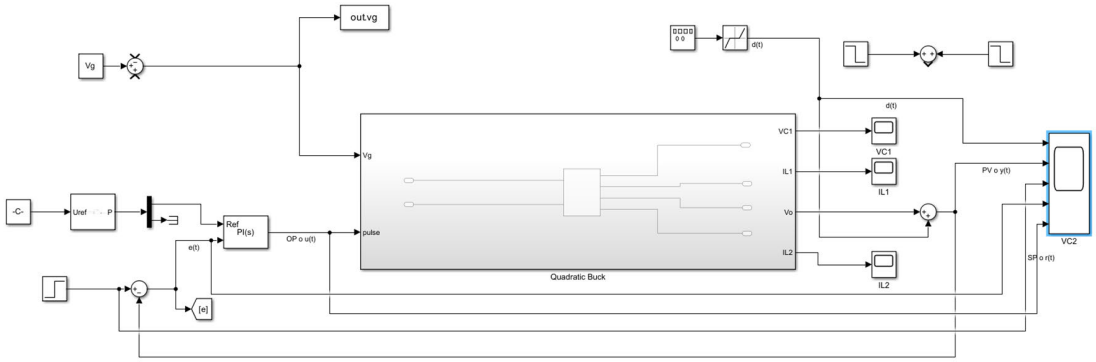

FIGURE 27. Passivity-based control model block diagram.

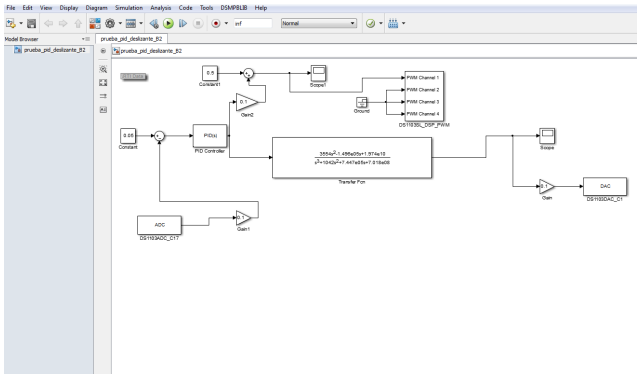

FIGURE 28. Double loop in slider mode for MATLAB application in dSPACE CP1103.

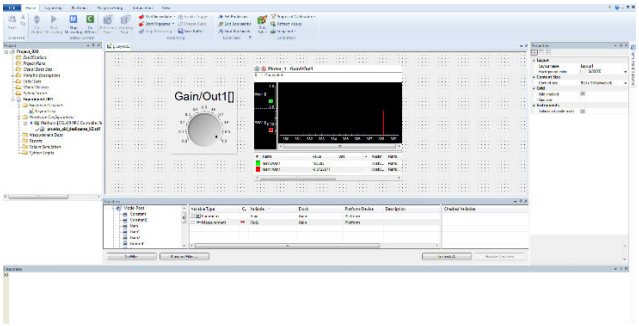

FIGURE 29. Signal response in control desk layout project.

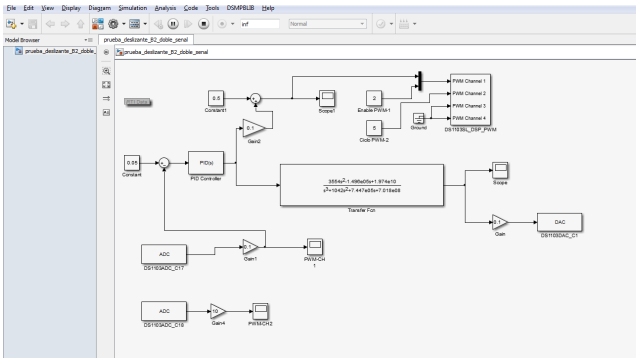

FIGURE 30. Dual input signal assignment.

the control in sliding mode control SMC, as it appears in Figure 28.

The experimental Project is carried out from the Embedded System controller board module from which the signal is reviewed in RT as can be seen in Figure 29.

The signal output is obtained through the pc controller board interface, in a BNC connection with ADC input and DAC output. Next, the output voltage signal is sent through the output BNC to the oscilloscope.

APPENDIX F
DESIGN WITH SLIDING MODE CONTROL SMC DISTURBANCES

Using the simulation in RT locating two input signals, as appears in Figure 30.

As a disturbance, the 500 Hz signal is added to the normal input signal, which is 100 kHz, obtaining a real-time response of the two phases, as shown in Figure 31, and finally,

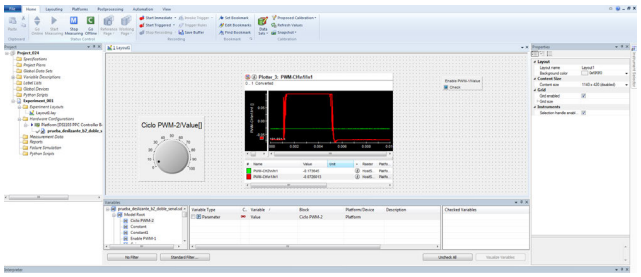

FIGURE 31. Signal action with a 500Hz disturbance.

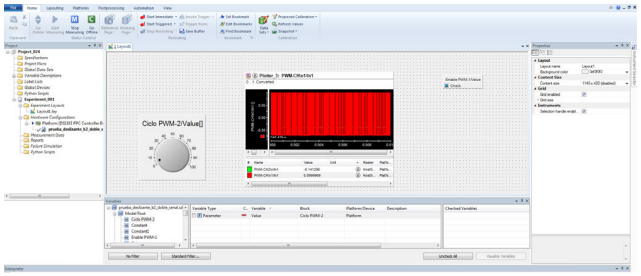

FIGURE 32. Input signals with 100HZ disturbance.

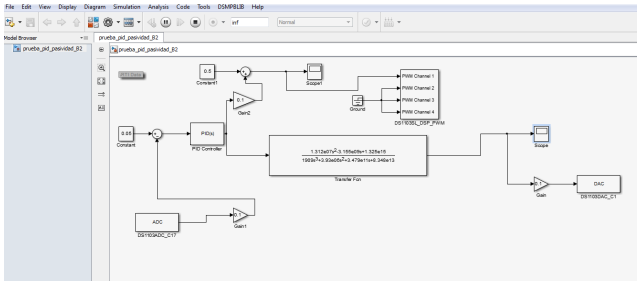

FIGURE 33. Passivity-based control PBC using a double supply loop.

FIGURE 34. Signal behavior with the signal in passive mode control. And the validation in oscilloscope.

the 100Hz disturbance signal, which superimposes that of 100KHz, as can be seen in figure 32.

APPENDIX G
EXPERIMENTAL CONTROL BY PASSIVITY-BASED CONTROL PBC

According to the design of the passive controller, the simulation is designed in Figure 33, the configuration of the passive signal is given in Figure 34, and the double-loop signal disturbance according to Figure 35.

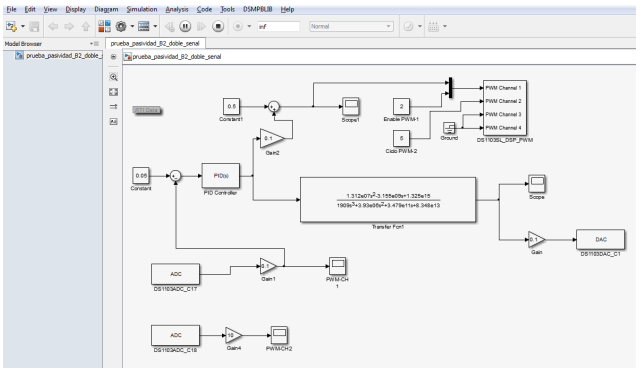

FIGURE 35. Dual signal input with disturbance.

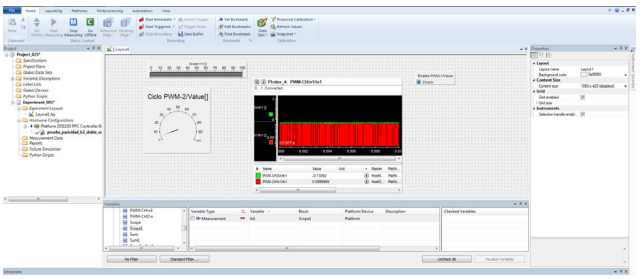

FIGURE 36. Control desk for two signals and one disturbance at 100HZ.

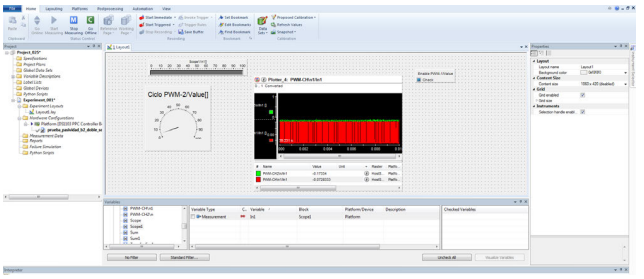

FIGURE 37. Control desk for two signals and one disturbance at 500HZ.

The double signal response is represented in the simulation. level.

Next, the configuration is carried out in Desk control of the double signal with a disturbance of 100HZ according to Figure 36.

Finally, for a 500HZ disturbance, the signal is defined by the Control Desk according to Figure 37.

REFERENCES

[1] M. Okati, M. Eslami, and M. J. Shahbazzadeh, "A new transformerless DC/DC converter with dual operating modes and continuous input current port," *IET Gener., Transmiss. Distrib.*, vol. 17, no. 7, pp. 1553–1567, Apr. 2023, doi: 10.1049/gtd2.12764.

[2] M. Okati, M. Eslami, M. J. Shahbazzadeh, and H. Shareef, "A new transformerless quadratic buck–boost converter with high-voltage gain ratio and continuous input/output current port," *IET Power Electron.*, vol. 15, no. 13, pp. 1280–1294, Oct. 2022, doi: 10.1049/pel2.12304.

[3] R. V. Damodaran, H. Shareef, R. Errouissi, and M. Eslami, "A common ground four quadrant buck converter for DC-AC conversion," *IEEE Access*, vol. 10, pp. 44855–44868, 2022, doi: 10.1109/ACCESS.2022.3169758.

[4] M. Okati, M. Eslami, and M. J. Shahbazzadeh, "A non-isolated DC–DC converter with dual working modes and positive output voltage," *Electr. Power Compon. Syst.*, vol. 49, nos. 13–14, pp. 1143–1157, Aug. 2021, doi: 10.1080/15325008.2022.2049662.

[5] J. M. Sosa, E. D. Silva-Vera, G. Escobar, P. R. Martinez-Rodriguez, and A. A. Valdez-Fernandez, "Control design for a quadratic buck converter with LC input filter," in *Proc. 13th Int. Conf. Power Electron. (CIEP)*, Guanajuato, Mexico, Jun. 2016, pp. 149–154, doi: 10.1109/CIEP.2016.7530747.

[6] S. Trakuldit, K. Tattiwong, and C. Bunlaksananusorn, "Design and evaluation of a quadratic buck converter," *Energy Rep.*, vol. 8, pp. 536–543, Apr. 2022, doi: 10.1016/j.egyr.2021.11.124.

[7] R. Xie, B. Liang, H. Zhang, and Y. Li, "A novel constant frequency sliding mode control for bidirectional quadratic boost-buck converter," in *Proc. IEEE Int. Conf. Ind. Technol. (ICIT)*, Melbourne, VIC, Australia, Feb. 2019, pp. 1663–1668, doi: 10.1109/ICIT.2019.8843695.

[8] K. Pandey, M. Kumar, A. Kumari, and J. Kumar, "Control of quadratic buck converter using non-linear controller," in *Proc. IEEE 17th India Council Int. Conf. (INDICON)*, New Delhi, India, Dec. 2020, pp. 1–6, doi: 10.1109/INDICON49873.2020.9342109.

[9] H. Nagy, M. Ruba, H. Hedesiu, and C. Martis, "Rapid control prototyping of a speed control strategy for a switched reluctance machine," in *Proc. Int. Conf. Exposit. Electr. Power Eng. (EPE)*, Iaşi, Romania, Oct. 2016, pp. 664–668.

[10] A. Sel, U. Gunes, and C. Kasnakoglu, "Output feedback discrete SMC design for quadratic buck DC–DC converter," in *Proc. 22nd Int. Conf. Syst. Theory, Control Comput. (ICSTCC)*, Sinaia, Romania, Oct. 2018, pp. 728–733, doi: 10.1109/ICSTCC.2018.8540665.

[11] I. A. Reyes-Portillo, J. A. Morales-Saldaña, E. M. Netzahuatl-Huerta, E. R. Palacios-Hernández, and S. R. Méndez-Elizondo, "Modeling of a quadratic buck converter based on the R2P2 concept for PV applications," in *Proc. IEEE Int. Autumn Meeting Power, Electron. Comput. (ROPEC)*, Ixtapa, Mexico, vol. 4, Nov. 2020, pp. 1–6, doi: 10.1109/ROPEC50909.2020.9258753.

[12] A. Mostaan, S. A. Gorji, M. Soltani, and M. Ektesabi, "A novel quadratic buck-boost DC–DC converter without floating gate-driver," in *Proc. IEEE 2nd Annu. Southern Power Electron. Conf. (SPEC)*, Auckland, New Zealand, Dec. 2016, pp. 1–5, doi: 10.1109/SPEC.2016.7846053.

[13] M. S. Ali, M. Soliman, A. M. Hussein, and S. A. F. Hawash, "Robust controller of buck converter feeding constant power load," *J. Control, Autom. Electr. Syst.*, vol. 32, no. 1, pp. 153–164, Feb. 2021, doi: 10.1007/s40313-020-00660-2.

[14] S. Ozdemir, N. Altin, and I. Sefa, "Fuzzy logic based MPPT controller for high conversion ratio quadratic boost converter," *Int. J. Hydrogen Energy*, vol. 42, no. 28, pp. 17748–17759, Jul. 2017.

[15] Ç. Hîsar, I. Sefa, and N. Altin, "Processor-in-the-loop simulation of an interleaved buck converter with MATLAB/simulink," in *Proc. 13th Int. Conf. Electron., Comput. Artif. Intell. (ECAI)*, Pitesti, Romania, Jul. 2021, pp. 1–6, doi: 10.1109/ECAI52376.2021.9515058.

[16] B. Baby and T. M. Abraham, "Bidirectional buck-boost quadratic converter using fuzzy controller for distributed generation systems," in *Proc. Int. Conf. Current Trends towards Converging Technol. (ICCTCT)*, Coimbatore, India, Mar. 2018, pp. 1–5, doi: 10.1109/ICCTCT.2018.8551025.

[17] A. Orozco and M. Isabel, "Nonlinear control of DC/DC switched converters: Performance analysis and experimental verification," Ph.D. thesis, Universitat Politécnica de Catalunya, 2007.

[18] C. A. Torres-Pinzón, F. Flores-Bahamonde, J. A. Garriga-Castillo, H. Valderrama-Blavi, R. Haroun, and L. Martínez-Salamero, "Sliding-mode control of a quadratic buck converter with constant power load," *IEEE Access*, vol. 10, pp. 71837–71852, 2022, doi: 10.1109/ACCESS.2022.3186312.

[19] L. B. Oliveira, J. C. Basilio, and R. C. L. F. Oliveira, "A survey on ITAE-based methods for optimal tuning of PID controllers," *J. Control, Autom. Electr. Syst.*, vol. 30, no. 3, pp. 323–341, Jun. 2019, doi: 10.1007/s40313-018-0447-4.

[20] R. Samiappan and V. Gomathy, "An analytical study of optimal controller design using ITAE and frequency response techniques for buck converter," *Int. J. Power Electron. Drive Syst.*, vol. 12, no. 2, pp. 141–152, Jun. 2021, doi: 10.11591/ijpeds.v12.i2.

[21] M.-H. Chang, F. Chen, and H.-S. Teng, "Effects of two-phase transport in the cathode gas diffusion layer on the performance of a PEMFC," *J. Power Sources*, vol. 160, no. 1, pp. 268–276, Sep. 2006, doi: 10.1016/j.jpowsour.2006.01.027.

[22] V. Vishal, V. Kumar, K. P. S. Rana, and P. Mishra, "Comparative study of some optimization techniques applied to DC motor control," in *Proc. IEEE Int. Advance Comput. Conf. (IACC)*, Gurgaon, India, Feb. 2014, pp. 1342–1347, doi: 10.1109/IADCC.2014.6779522.

[23] A. Goudarzian and A. Khosravi, "Voltage-controlled quadratic buck converter for a DC power management system with constant current load," *J. Control, Autom. Electr. Syst.*, vol. 31, no. 1, pp. 153–164, Feb. 2020, doi: 10.1007/s40313-019-00504-8.

[24] V. M. Pacheco, A. J. do Nascimento Jr., V. J. Farias, J. B. Vieira, and L. C. de Freitas, "A quadratic buck converter with lossless commutation," *IEEE Trans. Ind. Electron.*, vol. 47, no. 2, pp. 264–272, Apr. 2000.

[25] A. Gad and M. Farooq, "Applications of fuzzy logic in engineering problems," in *Proc. 27th Annu. Conf. IEEE Ind. Electron. Soc.*, Denver, CO, USA, Nov./Dec. 2001, pp. 2044–2049.

[26] R. W. Erickson and D. Maksimovic, *Fundamentals of Power Electronics*, 2nd ed. Norwell, MA, USA: Kluwer, 2001.

[27] J. A. Morales-Saldana, J. Leyva-Ramos, E. E. Carbajal-Gutierrez, and M. G. Ortiz-Lopez, "Average current-mode control scheme for a quadratic buck converter with a single switch," *IEEE Trans. Power Electron.*, vol. 23, no. 1, pp. 485–490, Jan. 2008.

[28] M. A. Al-Saffar, "Integrated buck–boost–quadratic buck PFC rectifier for universal input applications," *IEEE Trans. Power Electron.*, vol. 24, no. 12, pp. 2886–2896, Dec. 2009.

[29] N. S. Nise, *Control Systems Engineering*, 5th ed. Hoboken, NJ, USA: Wiley, 2006.

[30] B. C. Kuo, *Automatic Control Systems*, 8th ed. Upper Saddle River, NJ, USA: Prentice-Hall, 2006.

[31] B. Friedland, *Control System Design*, 2nd ed. Boca Raton, FL, USA: Taylor & Francis, 2008.

[32] G. F. Franklin, J. D. Powell, and A. Emami-Naeini, *Feedback Control of Dynamic Systems*, 6th ed. Upper Saddle River, NJ, USA: Prentice-Hall, 2006.

[33] A. Ghosh, S. Banerjee, M. K. Sarkar, and P. Dutta, "Design and implementation of type-II and type-III controller for DC–DC switched-mode boost converter by using K-factor approach and optimisation techniques," in *IEEE Access*, vol. 8, pp. 158486–158494, 2020.

[34] M. R. Islam, "Demystifying type II and type III compensators using OpAmp and OTA for DC/DC converters," *IEEE Access*, vol. 7, pp. 1–8, 2019, doi: 10.1109/ACCESS.2019.2946746.

[35] V. Utkin, "Sliding mode control and observers," *IEEE Trans. Autom. Control*, vol. 37, no. 2, pp. 132–137, 1992.

[36] M. S. Branicky, "Sliding mode control of linear systems," *IEEE Trans. Autom. Control*, vol. 39, no. 2, pp. 246–251, 1994.

[37] C. Edwards and S. K. Spurgeon, *Sliding Mode Control*. London, U.K.: Taylor & Francis, 1998.

[38] R. Ortega, A. Loria, H. Nicklasson, and H. Sira-Ramírez, *Passivity-Based Control of Euler–Lagrange Systems: Mechanical, Electrical, and Electromechanical Applications*. London, U.K.: Springer, 1998.

[39] M. Fliess, "Generalized controller canonical form for linear and nonlinear dynamics," *IEEE Trans. Autom. Control*, vol. 35, no. 9, pp. 994–1001, Sep. 1990.

[40] C. L. Phillips and H. T. Nagle, *Digital Control System: Analysis and Design*, Upper Saddle River, NJ, USA: Prentice-Hall, 1990.

[41] D. C. Montgomery, *Statistical Processes Control*, New York, NY, USA: McGraw-Hill, 2010.

[42] K. Ishikawa, *Quality and Productivity in the Industry*. Upper Saddle River, NJ, USA: Prentice-Hall, 1988.

[43] D. C. Montgomery, *Introduction to Statistical Quality Control*. Hoboken, NJ, USA: Wiley, 2013.

[44] P. Viana, *Industrial Process Control*, 3rd ed. Madrid, Spain: Pearson, 2015.

[45] J. Fei, Z. Wang, and Q. Pan, "Self-constructing fuzzy neural fractional-order sliding mode control of active power filter," *IEEE Trans. Neural Netw. Learn. Syst.*, pp. 1–12, 2022, doi: 10.1109/TNNLS.2022.3169518.

[46] J. Fei and L. Liu, "Fuzzy neural super-twisting sliding-mode control of active power filter using nonlinear extended state observer," *IEEE Trans. Syst., Man, Cybern. Syst.*, vol. 54, no. 1, pp. 457–470, Jan. 2024, doi: 10.1109/TSMC.2023.3310593.

[47] J. Fei, L. Zhang, J. Zhuo, and Y. Fang, "Wavelet fuzzy neural supertwisting sliding mode control of an active power filter," *IEEE Trans. Fuzzy Syst.*, vol. 31, no. 11, pp. 4051–4063, Nov. 2023, doi: 10.1109/TFUZZ.2023.3272028.

RAFAEL ANTONIO ACOSTA-RODRÍGUEZ (Member, IEEE) received the bachelor's degree in electronic engineering and the Specialist degree in teleinformatics from Universidad Distrital Francisco José de Caldas, Colombia, in 2002 and 2016, respectively, and the master's degree in mechatronic engineering from Universidad Militar Nueva Granada, Colombia, in 2016. He is currently pursuing the Ph.D. degree in engineering with an emphasis in electrical and electronic engineering. His research in the intelligent internet and ARMOS Groups, categorized in A1 Colciencias, Colombia.

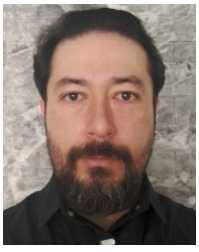

FREDY HERNÁN MARTINEZ-SARMIENTO (Member, IEEE) received the Ph.D. degree in computer and systems engineering from Universidad Nacional de Colombia. He is currently a Professor in control, intelligent systems, power converters, and robotics with Universidad Distrital Francisco José de Caldas, Colombia. He leads the ARMOS Research Group, dedicated to the innovation of modern architectures for power systems. His scholarly pursuits predominantly encompass control strategies for power converters, autonomous robotics, mathematical modeling, electronic instrumentation, comprehensive pattern recognition, and the exploration of multi-agent systems.

GERMAN ARDUL MÚÑOZ-HERNANDEZ (Senior Member, IEEE) received the B.Sc. degree in electronic engineering from the Veracruz Institute of Technology, in 1988, the M.Sc. degree in electronic systems from the National Institute of Astrophysics Optics and Electronics, in 1990, and the Ph.D. degree from the University of Wales, Bangor, in 2005. He was with FAPATUX, Tuxtepec, Mexico, from 1986 to 1987, and from 1990 to 1993. He has been a Visiting Engineer at Columbia, SC, USA, since 1995; Ann Arbor, MI, USA, in 1996; and the CERN, Geneva, Switzerland, in 2007 and 2009. His main research interests include control systems applications and automation. He is a Senior Member of the Level II of the National Systems of Researchers, Mexico.

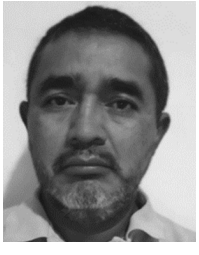

GERARDO MINO-AGUILAR (Senior Member, IEEE) was born in Mexico, in 1971. He received the bachelor's degree in electronics engineering from Meritorious Autonomous University of Puebla (BUAP), Puebla, Mexico, in 1998, the M.S. degree in electronics engineering from Universidad de las Américas Puebla, Cholula, Mexico, in 1998, and the Ph.D. degree in electrical engineering from Universitat Politècnica de Catalunya, Barcelona, Spain, in 2007. He is currently the Head of the Postgraduate and Research Department, Faculty of Electronics Sciences, BUAP. His research interests include power electronics, electric drives, power quality, electric vehicles, and motion control.

EDGAR ALFREDO PORTILLA-FLORES (Member, IEEE) was born in Tlaxcala, Mexico, in 1968. He received the B.Sc. degree in electronics engineering from Universidad Autónoma Metropolitana, Mexico, in 1992, the M.Sc. degree in mechanical engineering from Instituto Tecnológico de Puebla, Mexico, in 2002, and the Ph.D. degree in electrical engineering from the Centro de Investigación y Estudios Avanzados, Mexico, in 2006. He completed the Postdoctoral Residency with Universidade Estadual de Campinas, Brazil, in 2012. He is currently a full-time Research Professor with Unidad Profesional Interdisciplinaria de Ingeniería Campus Tlaxcala, Instituto Politécnico Nacional, Mexico. His research interests include the optimum design of mechatronic systems and the application of bio-inspired algorithms to the solution of engineering problems. He is a member of the National System of Researchers of Mexico.

PAOLA ANDREA NIÑO-SUAREZ (Member, IEEE) received the B.Sc. degree in electronics engineering from Universidad Antonio Nariño, Colombia, in 1995, the M.Sc. degree in electrical engineering biomedical specialty from Universidad de Los Andes, Colombia, in 1998, and the Ph.D. degree in electrical engineering from the Centro de Investigación y de Estudios Avanzados del Instituto Politécnico Nacional (IPN), Mexico, in 2006. She is currently a Researcher and a Professor with the Sección de Estudios de Posgrado e Investigación, Escuela Superior de Ingeniería Mecánica y Eléctrica Azcapotzalco, IPN, Mexico. Her research interests include mechatronics and mobile robotics.

OCTAVIO JOSÉ SALCEDO-PARRA (Member, IEEE) received the bachelor's degree in system engineering and the master's degree in teleinformatics from Universidad Distrital Francisco José de Caldas, Colombia, and the Ph.D. degree from the Pontifical University of Salamanca. He is currently a Research Professor in the doctorate of engineering with Universidad Distrital Francisco José de Caldas. He is also the Research Director with the Intelligent Internet Group, categorized in A1 Colciencias, Colombia.